Ultradian rhythms in shell composition of photosymbiotic and non-photosymbiotic mollusks

Niels J. de Winter[1,2], Daniel Killam[3], Lukas Fröhlich[4], Lennart de Nooijer[5], Wim Boer[5], Bernd R. Schöne[4], Julien Thébault[6], Gert-Jan Reichart[5,7]

Affiliations

[1]Dept. of Earth Sciences, Vrije Universiteit Amsterdam, Amsterdam, the Netherlands

[2]Analytical, Environmental and Geochemistry group (AMGC), Vrije Universiteit Brussel, Brussels, Belgium

[3] San Francisco Estuary Institute, Richmond, CA, USA

[4] Institute of Geosciences, University of Mainz, Germany

[5] Dept. of Ocean Systems, Royal Netherlands Institute for Sea Research (NIOZ), Texel, the Netherlands

[6]Univ Brest, CNRS, IRD, Ifremer, LEMAR, 29280 Plouzané, France, (ORCID: 0000-0002-3111-4428)

[7]Dept. of Earth Sciences, Utrecht University, Utrecht, the Netherlands

Corresponding author: N.J. de Winter, n.j.de.winter@vu.nl

Abstract

The chemical composition of mollusk shells is a useful tool in (paleo)climatology since it captures inter- and intra-annual variability in environmental conditions. Trace element and stable isotope analysis with improved sampling resolution now allows *in-situ* determination of the composition of mollusk shell volumes precipitated at daily to sub-daily time intervals. Here, we discuss hourly resolved Mg/Ca, Mn/Ca, Sr/Ca and Ba/Ca profiles measured by laser ablation ICP-MS through shells of photosymbiotic giant clams (*Tridacna maxima*, *T. squamosa* and *T. squamosina*) and the non-photosymbiotic scallop *Pecten maximus*. Precise sclerochronological age models and spectral analysis allowed us to extract daily and tidal rhythms in the trace element composition of these shells. We find weak but statistically significant expression of these periods and conclude that this cyclicity explains less than 10 % of the sub-annual variance in trace element profiles. Tidal and diurnal rhythms explain variability of at most 0.2 mmol/mol (~10 % of mean value) in Mg/Ca and Sr/Ca, while ultradian Mn/Ca and Ba/Ca cyclicity has a median amplitude of less than 2 µmol/mol (~ 40 % and 80 % of the mean of Mn/Ca and Ba/Ca, respectively). Daily periodicity in Sr/Ca and Ba/Ca is stronger in *Tridacna* than in *Pecten*, with *Pecten* showing stronger tidal periodicity. One *T. squamosa* specimen which grew under a sunshade exhibits among the strongest diurnal cyclicity. Daily cycles in trace element composition of giant clams are therefore unlikely to be driven by variations in direct insolation, but rather reflect an inherent biological rhythmic process affecting element incorporation. Finally, the large amount of short-term trace element variability unexplained by tidal and daily rhythms highlights the dominance of aperiodic processes in mollusk physiology and/or environmental conditions on shell composition at the sub-daily scale. Future studies should aim to investigate whether this remaining variability in shell chemistry reliably records weather patterns or circulation changes in the paleoenvironment.

1. Introduction

45 Patterns in growth increments, microstructure, and chemical composition of accretionary

46 carbonate bioarchives yield detailed information about the environmental conditions and

47 biological rhythm of carbonate producing animals (Dunbar and Wellington, 1981; Jones, 1983;

48 Witbaard et al., 1994; Klein et al., 1996; Surge et al., 2001; Schöne et al., 2005a; Ivany, 2012;

49 Schöne and Gillikin, 2013; DeCarlo and Cohen, 2017; Killam and Clapham, 2018a). These

50 characteristics have spurred the development of a multitude of techniques for extracting

51 information about life history (Jones and Quitmyer, 1996; Schöne et al., 2005b; Eggins et al.,

52 2003; Anand and Elderfield, 2005; Goodwin et al., 2009; Mahé et al., 2010; Comboul et al., 2014;

53 DeCarlo and Cohen, 2017; Judd et al., 2018; Winter et al., 2022), carbonate chemistry (Sinclair

54 et al., 1998; Lazareth et al., 2003; Schöne et al., 2010; de Winter and Claeys, 2017; Warter and

55 Müller, 2017; Huyghe et al., 2021; de Winter et al., 2021b) and microstructure (Lazier et al., 1999;

56 Checa et al., 2007; Popov, 2014; Gilbert et al., 2017; Crippa et al., 2020; Höche et al., 2020, 2021;

57 Wichern et al., 2022) from carbonate shells and skeletons. As a result, (fossil) carbonate

58 skeletons have gained much attention as archives of past environmental and climate change

59 (Lough, 2010; Schöne and Gillikin, 2013; Ivany and Judd, 2022) and references therein).

60 Three characteristics make the shells of marine mollusks especially valuable as climate archives:

61 (1) Nearly all marine mollusks precipitate their shells in equilibrium with the oxygen isotope value

62 of ambient sea water, except for juvenile oysters, some mollusks growing near hydrothermal vents

63 and some deep-burrowing species (Schöne et al., 2004; Hallmann et al., 2008; Wisshak et al.,

64 2009; Huyghe et al., 2021; de Winter et al., 2022), (2) mollusk shells have a high fossilization

65 potential and long geological history, dating back to the beginning of the Phanerozoic (Al-Aasm

66 and Veizer, 1986a, b; Jablonski et al., 2003; Cochran et al., 2010; Jablonski et al., 2017; de Winter

67 et al., 2017, 2018; Coimbra et al., 2020), (3) the incremental growth of mollusk shells allows for

68 internal dating within the shell, yielding chronologies of shell growth with sub-annual precision

69 (Richardson et al., 1980; Jones, 1983; Schöne et al., 2005b; Goodwin et al., 2009; Huyghe et al.,

70   2019). These advantages enable mollusk shells to record important information about climate and

71   ambient water chemistry on the seasonal scale. Thereby, reconstructions from mollusk shells are

72   highly complementary to other, less highly resolved but longer-term, climate and environmental

73   reconstructions like sedimentary records, tree rings and ice cores (Black, 2009; Bougeois et al.,

74   2014; Petersen et al., 2016; Tierney et al., 2020; de Winter et al., 2021a).

75   The resolution of the mollusk shell archive is not limited to seasonal variability. Studies monitoring

76   the behavior of mollusks during growth experiments show that their activity varies as a function

77   of environmental conditions (e.g., temperature and food availability) and follows ultradian rhythms

78   which may contain daily to hourly periodicities, probably linked to diurnal and tidal cycles, or lack

79   periodic behavior altogether (Rodland et al., 2006; García-March et al., 2008; Tran et al., 2011;

80   Ballesta-Artero et al., 2017; Xing et al., 2019; Tran et al., 2020). Analyses of growth patterns and,

81   more recently, composition of shell carbonate deposited at these short time intervals show that

82   these rhythms can be recorded in mollusk shells (Pannella, 1976; Richardson et al., 1980; Sano

83   et al., 2012; Warter et al., 2018; de Winter et al., 2020). This raises the question whether mollusk

84   shells reliably record behavioral changes, high frequency (paleo-)weather or circulation patterns

85   (e.g. (Komagoe et al., 2018; Yan et al., 2020; Poitevin et al., 2020). Alternatively, the presence of

86   daily cyclicity in shell chemistry may yield information about the paleobiology of extinct mollusks,

87   such as the use of photosymbiosis (e.g. (Sano et al., 2012; Warter et al., 2018; de Winter et al.,

88   2020). The latter seems plausible given the effect of photosymbiosis on shell mineralization in

89   modern tridacnids (Ip and Chew, 2021) and on the trace element composition of aragonite in

90   modern photosymbiotic scleractinian corals (Cohen et al., 2002; Meibom et al., 2003; Inoue et al.,

91   2018). If proven true, daily variability in bivalve shells may serve as a proxy for photosymbiosis in

92   the fossil record (e.g. (de Winter et al., 2020). This is of interest because photosymbiosis is a

93   derived adaptation of some tropical bivalve species (e.g., tridacnids) and its prevalence in the

94   fossil record has important implications for the ecological niche of fossil mollusks (e.g. (Vermeij,

2013)). In addition, photosymbiosis can affect mollusk shell composition, and understanding it is therefore critical for the interpretation of chemical proxies in mollusk shells for environmental reconstructions (Killam et al., 2020). Finally, improving our understanding of photosymbiosis in tropical ecosystems sheds light on the resilience of photosymbiotic organisms to environmental change, now and in the geological past. The latter is of special interest in light of the ongoing climate and biodiversity crises, which are profoundly affecting these sensitive ecosystems (Pandolfi and Kiessling, 2014).

In this study, we investigate shell growth patterns and shell chemistry of the photosymbiotic bivalves *Tridacna maxima*, *T. squamosa* and *T. squamosina* as well as the non-photosymbiotic scallop *Pecten maximus*. *P. maximus* was chosen as a non-photosymbiotic counterpart in comparison with the tridacnids because of its comparatively high growth rate and the presence of daily striae visible on the outer surface of its shell, which make it possible to construct accurate shell chronologies (Chauvaud et al., 2005). We combine ultra-high-resolution (hourly resolved) Mg/Ca, Sr/Ca, Mn/Ca and Ba/Ca measurements in the shells with detailed sclerochronology to investigate the variability in these trace elements over time in all four species. The aim of this study is to investigate (1) whether the shells record high-frequency variability in shell chemistry that can be linked to environmental and/or circadian rhythms and (2) whether the presence of photosymbiosis influences the expression of this variability in the shells' composition.

2. Materials and methods

2.1 Preparation of *P. maximus* specimens

Three specimens of the King scallop *P. maximus* (labeled "**PM2**", "**PM3**" and "**PM4**") were collected alive on 15/11/2019 on the southern coast of the Bay of Brest near Lanvéoc, France (48°17′N 4°30′W) by SCUBA divers at a depth of approximately 8 m (see (Fröhlich et al., 2022); **Figure 1**). Note that water depth in the Bay of Brest varies significantly due to the macrotidal regime with a mean tidal range of 2.8 – 5.9 m with extreme ranges up to 7.2 m (Guillaume Olivier et al., 2021; Service Hydrographique et Océanographique de la Marine - Géoportail, 2022). Collected specimens contained at least one full year of growth based on the visibility of one winter growth line on the outside of the shell (age class 1; see (Thébault et al., 2022); **Fig 1F** and **S1**). Specimens were frozen at -20°C immediately after collection. Soft body parts and epibionts were removed from the shells before further treatment. Shells were superficially cleaned using a plastic brush and adhering sediment was removed by ultrasonication in deionized water. The flat, left valves were used for elemental and sclerochronological analysis following previous studies on *P. maximus* (Thébault et al., 2022; Fröhlich et al., 2022).

High-resolution color photos were made of the outside of the left valve of the shell using a mirror-reflex camera (Canon EOS 600 DSLR camera connected to a Wild Heerbrugg binocular microscope equipped with a Schott VisiLED MC 1000 sectoral dark-field light source) aimed downward perpendicular to the working surface. Overlapping images of the shells were stitched together using Image Composite Editor v2.0.3.0 (Microsoft Research Computational Photography Group, Redmond, WA, USA). The stitched images were used to count and measure daily striae on the shell surface (see **Fig. 1** and **S1**). To obtain a fully focused composite of the complete shell, dynamic focusing was applied to allow all parts of the slightly curved surface of the shell to come into focus. Dynamic focus images where later stitched together using focus stacking in Helicon Focus (Helicon Focus 7.7.5; HeliconSoft, Kharkiv, Ukraine; see **S1**).

139 Cross sections were cut through all three *P. maximus* shells perpendicular to the daily growth

140 lines (striae) from the ventral margin of the shell to the shell hinge (see **Fig. 1B-D** and **S1**) along

141 the axis of maximal growth. Shells were fortified with a protective layer of metal epoxy (Gluetec

142 Wiko Epofix 05) before sectioning using a Buehler Isomet 1000 low-speed precision saw (Buehler

143 Inc, Lake Bluff, IL, USA) equipped with a diamond-coated wafering thin blade (0.4 mm thickness;

144 number 15LC 11–4255) at 200 rpm. Parallel cuts were made to allow shell sections to be glued

145 to glass plates for grinding (down to F1200 grit SiC powder) and high-grade polishing (1 μm Al_2O_3

146 suspension on Buhler polishing cloth, MasterTex). Two cross sections were made through

147 specimens **PM2** and **PM3**: One through a "rib" of the shell (i.e., radial segment that protrudes

148 away from the interior, named **PM2_1** and **PM3_1**) and one through a "valley" (i.e., radial segment

149 between two "ribs" that lies deeper towards the interior, named **PM2_2** and **PM3_2**; see **Fig. 1**

150 and **S1**). The dual sections were cut to compare shell chemistry between the "ribs" and "valleys"

151 of the shell. Specimen **PM4** was only sectioned once, through a "valley" in the shell, making a

152 total of five cross sections through the *P. maximus* specimens.

153

154
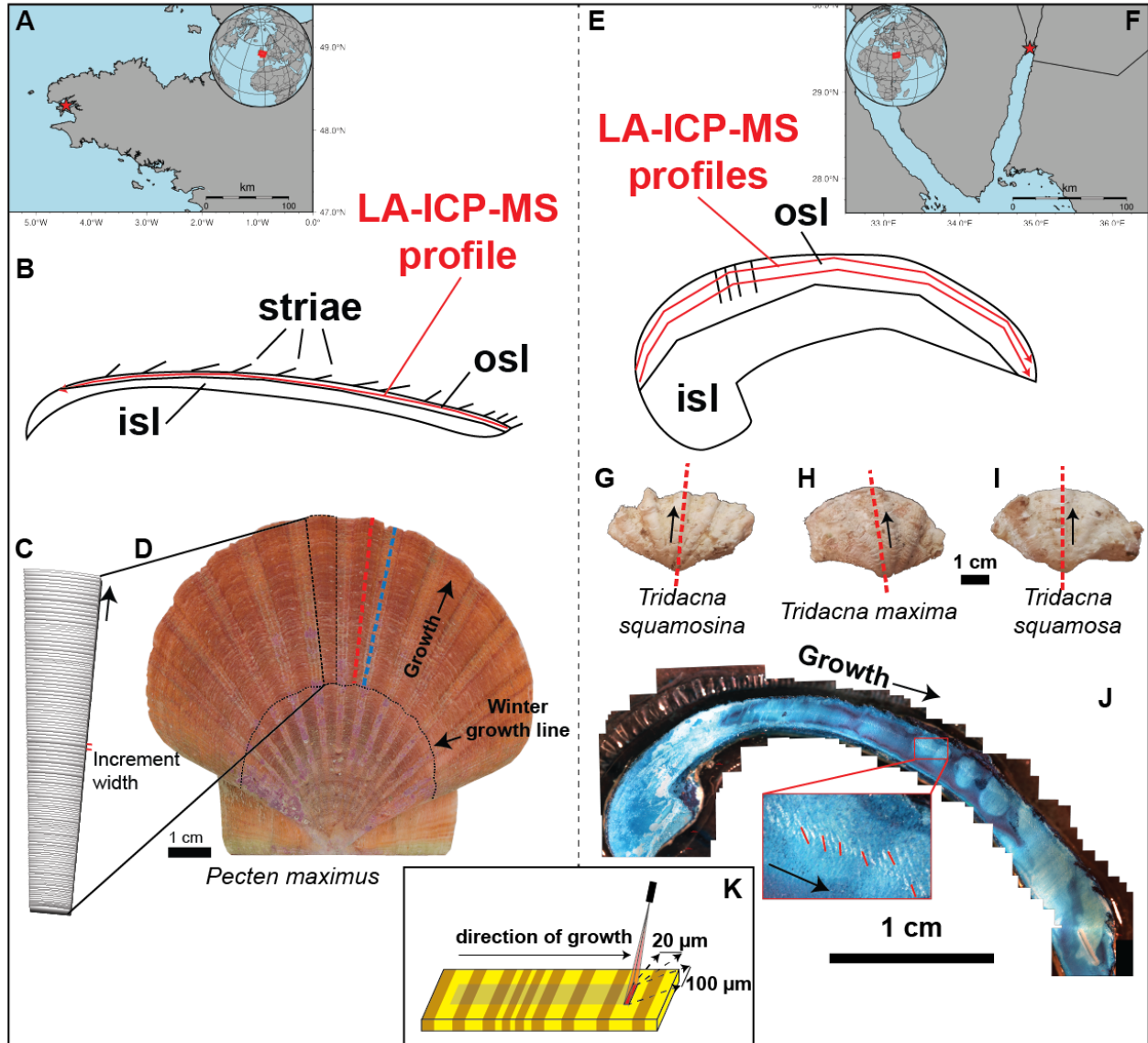
Figure 1: **Overview of sample locations and preparation steps**. **A)** Location of the Bay of Brest, with the red star indicating the sampling location. **B)** Schematic cross section through *P. maximus* showing how the LA-ICP-MS line scan (red line) was positioned within the outer shell layer (OSL).**C)** Schematic representation of a segment through the shell of *P. maximus* showing the striae which are deposited daily and which were counted to establish age models (see also **B**). **D)** Left valve of *P. maximus* (**PM2**) used in this study, with dashed lines showing the position of cross sections through ribs (red) and valleys (blue) in the shell. Black arrow indicates growth direction away from the shell hinge. The black dotted line highlights a winter growth stop. **E)**

163   Schematic cross section through a tridacnid, illustrating the positions of parallel LA-ICP-MS line

164   scans (red lines) through these shells within the OSL. **F)** Position of the Gulf of Aqaba, with the

165   red star indicating the sample location for tridacnids. **G-I)** Pictures of (from left to right) *T.*

166   *squamosa* (specimen **TSFRS1**), *T. maxima* (specimen **TM29**) and *T. squamosina* (specimen

167   **SQSA1**) with dashed red lines indicating the positions of the cross sections used for LA-ICP-MS

168   analysis (see **C**) and black arrows indicating the direction of growth. **J**) Example of Mutvei-stained

169   cross section through a *T. maxima* specimen used to visualize and count growth lines, with the

170   insert showing part of the OSL where growth lines were counted (red lines) to establish age

171   models for the tridacnids. Black arrows indicate the direction of growth. **K)** Schematic

172   representation of the LA-ICP-MS line scanning setup with the rectangular spot size (100 * 20 μm;

173   see **S11**) that was positioned parallel to the growth layers in the shell.

174

175   2.2 Preparation of *Tridacna* specimens

176   A total of 5 tridacnid specimens, two *T. maxima* (named **TM29** and **TM84**), two *T. squamosa*

177   (named **TS85** and **TSFRS1**) and one *T. squamosina* (**SQSA1**) specimen, were collected in the

178   summer of 2016 from beach death assemblages on the coast of the Gulf of Aqaba with permit

179   from the Israeli National Parks Authority (**Figure 1**; see details in (Killam et al., 2020)). One

180   cultured *Tridacna squamosa* shell (**TSM1**) was obtained from the National Center for Mariculture,

181   Eilat. Species were determined following shell characteristics of the local population as cited in

182   (Roa-Quiaoit, 2005).

183   All shells were sectioned along the axis of maximum growth after removing epibionts using a

184   metal brush (see **Fig. 1G-I**). Original microstructure and preservation of the original aragonite

185   mineralogy of all specimens was confirmed using Scanning Electron Microscopy and X-ray

186   Diffraction Spectroscopy following (Gannon et al., 2017) and (Kontoyannis and Vagenas, 2000)

187   (see details in (Killam et al., 2020)). Shell segments were partially embedded in Araldite 2020

188   epoxy resin (Huntsman Corp., Woodlands, TX, USA) before being sectioned in direction of

189   maximum growth using a slow-rotating saw equipped with a thin wafered saw blade (ø < 1 mm).

190   Parallel cross sections produced 5-10 mm thick sections that were polished using progressively

191   finer SiC polishing disks.

192

193   2.3 Microscopy and photography

194   Polished surfaces of all 11 cross sections (5 *Pecten*, 6 *Tridacna*) were imaged using an Epson®

195   1850 flatbed scanner (Seiko Epson Corp., Nagano, Japan) at a pixel resolution of 6400 dpi (±4

196   µm pixel size) as well as by stitching micrographs made using a KEYENCE VHX-5000 digital

197   microscope using x250 magnification together into composite images (see **S1**). Cross sections

198   were imaged both before and after trace element analyses to allow the trace element profiles to

199   be referenced relative to the cross sections.

200

201   2.4 LA-ICP-MS analyses

202   Elemental ratios were based on measuring ratios of the isotopes ^{25}Mg, ^{87}Sr, ^{55}Mn and ^{137}Ba to

203   ^{43}Ca along profiles through all shell cross sections using Laser Ablation – Inductively Coupled

204   Plasma – Mass Spectrometry (LA-ICP-MS). Measurements were carried out on a laser ablation

205   system (ESI NWR193UC; Elemental Scientific, Omaha, NE, USA) coupled to a quadrupole ICP-

206   MS (iCap-Q, Thermo Fisher Scientific, Waltham, MA, USA) at the Royal Netherlands Institute for

207   Sea Research (NIOZ). Operation parameters are provided in **S11**.

208   Scan lines were programmed on the polished shell cross-sections in direction of growth as close

209   as possible to the outer edge of the shell, with the circular LA-ICP-MS spot oriented parallel to

210   the growth lines (with a width of 20 µm in scanning direction, see **Fig. 1J**; **S11**). For the pectinids,

211   care was taken to target the outer portion of the outer shell layer (oOSL) and avoid sampling of

212   the inner portion of the outer shell layer (iOSL) or inner shell layer (ISL), which was demonstrated

213   to have a different chemical composition (see Freitas et al., 2009). For the tridacnids, profiles

214   were placed within the OSL close to (within 100 µm of) the outer edge of the shell in a first

215   analytical session. However, since spikes of high Mg/Ca and Mn/Ca ratios were observed in these

216   results, parallel transects placed ~ 100 µm further towards the inside of the shell were measured

217   through all tridacnid shells to verify whether these spikes in Mg and Mn were reproducible further

218   inward (see **S2**). The combination of laser scan speed (4 µm * s^{-1}) and ICP-MS run cycle time

219   ("sweep time"; 109 ms) yielded a mean spatial sampling resolution of 0.44 µm, determined as the

220   arithmetic mean without taking into account the round shape of the laser spot. However, note that

221   the width of the LA-ICP-MS spot size in scanning direction (20 µm) caused smoothing of the LA-

222   ICP-MS signal, reducing the effective spatial sampling resolution. As a result, each 0.44 µm wide

223   segment of the shells in growth direction is sampled 45 times while the spot moves across the

224   shell. We tested the effect of this smoothing on a virtual record with characteristics similar to the

225   Sr/Ca record obtained by (Sano et al., 2012) (see **section 3.3** and **S13**). All scan lines in pectinids

226   and tridacnids were repeated a second time at the exact same location using a faster scan rate

227   of 10 µm * s^{-1} to assess repeatability of the elemental signals (see **S2**).

228   Data reduction was performed using an adapted version of the data reduction software SILLS

229   (Signal Integration for Laboratory Laser Systems; (Guillong et al., 2008)) in Matlab. Raw LA-ICP-

230   MS data were calibrated using NIST610, (National Institute of Standards and Technologies,

231   Gaithersburg, MD, USA) using the reference values reported in the GeoReM database (Jochum

232   et al., 2005, 2011). Quality control reference materials BAS CRM 393 (Bureau of Analyzed

233   Samples, Middlesbrough, UK), RS3 and one matrix-matched carbonate standard (MACS-3;

234   United States Geological Survey, Reston, VA, USA; (Wilson et al., 2008)) were used to monitor

235   the quality of the measurement. Details on the accuracy of the LA-ICP-MS trace element results

236   relative to preferred values for the check standards is provided in **S12**.

237   To increase the stability of the ICP-MS signal and to correct for drift, ^{43}Ca was used as internal

238   standard. Calcium concentrations were assumed to be constant (38 wt%) throughout the

239   LAICPMS profiles within the same shell layer. External drift-correction using repeated

240   measurements on the JCp1 standard was applied. The element/Ca drift was less than 5 % during

241   the analytical sequence. Drift during a single transect was found to be negligible.

242

243   2.5 Age models

244   Trace element profiles in *P. maximus* shells were internally dated using daily striae visible on the

245   outer shell surface (**Fig. 1D**). Daily increment widths (perpendicular distances between

246 successive striae) were counted and measured multiple times, both on the outside of the shell

247 using the focus-stacked images (see **section 2.3**) and by counting and measuring the distance

248 between growth layers in cross sections through the "valleys" of the shells (**PM2_2** and **PM3_2**;

249 see **S3**) by different persons. Positions of daily striae on the outside of the shells were plotted

250 relative to distance along the LA-ICP-MS scan line using manual alignment of striae and the LA-

251 ICP-MS path on microscope composites of cross sections through the shells, taking into account

252 the curvature of growth lines with distance away from the outer shell surface (see **S3**). The timing

253 of shell formation was determined by backdating the daily striae from the ventral margin (last

254 visible stria mineralized on the date of shell collection, i.e., November 15, 2019), and by linearly

255 interpolating the timing of measurements located between daily growth lines based on their

256 distance from daily striae positions (**S5**).

257 Trace element profiles from *Tridacna* shells were also dated using layer counting. Polished cross

258 sections through all tridacnids were imaged using UV luminescence (see **Fig. 1J** and **S4**) and

259 stained with Mutvei solution (Schöne et al., 2005c; Killam et al., 2021) to facilitate this counting.

260 However, despite staining and luminescence techniques, the expression of daily and semi-diurnal

261 (half-daily, or 12 h rhythmic) growth markings were insufficiently clear to count individual growth

262 lines along the full (multi-year) growth period recorded in all the shells. Therefore, we opted for a

263 hybrid method in which we measured the width of daily and semi-diurnal increments in parts of

264 cross sections of each shell where they were well developed and used these measurements in

265 combination with the annual growth breaks (which are easily recognized on the shell) to create

266 age models for all specimens. The distinction between diurnal (24 h) and tidal (~12 h) pacing of

267 growth increments was made based on the width of small-scale increments relative to the width

268 of annual increments in the shell. A von Bertalanffy growth model (Von Bertalanffy, 1957) was

269 constructed for each specimen based on the annual growth (ΔL) inferred from (semi-)diurnal

270   growth line counting and the maximum shell height (L_{inf}) known for these species in the Red Sea

271   from the literature (Roa-Quiaoit, 2005; Mohammed et al., 2019):

272    $$L_t = L_{inf} * \left(1 - e^{-kt}\right), with\ k = -ln\left(\frac{\Delta L}{L_{inf}}\right)$$

273   In this formula, L_t is the shell height at time t and k is the growth constant (Brody growth coefficient;

274   (Munro, 1982)). Since cross sections through the tridacnids were made through the shell hinge

275   (in direction of the shell height) and literature values for L_{inf} are reported with reference to shell

276   length (measured parallel to the shell hinge), allometric data on *T. maxima*, *T. squamosa* and *T.*

277   *squamosina* from the literature was used to convert L_{inf} values (which are commonly reported as

278   shell length) to shell height and make them relevant for the direction in which the trace element

279   profiles were measured on the cross sections (Roa-Quiaoit, 2005; Richter et al., 2008;

280   Mohammed et al., 2019). Uncertainties on the annual growth increment widths (ΔL) were

281   calculated from the standard error of the mean width of daily and semi-diurnal growth increments

282   on which ΔL is based, and uncertainties on the values for L_{inf} were taken from variability in the

283   values in the literature. Both sources of uncertainty were propagated through the growth model

284   using the variance formula (Ku, 1966) to obtain error envelopes on age-distance relationships

285   (growth curves) of tridacnids (see **S5**). All data processing steps described in this manuscript are

286   carried out using the open-source computational software package R (R Core Team, 2013), and

287   scripts detailing these calculations are provided in **S6** and deposited on the open-access software

288   repository GitHub (https://zenodo.org/record/6603175)

289

290   2.6 Spectral analysis

291   Spectral analysis on the LA-ICP-MS data was used to isolate trace element variability at the sub-

292   annual scale. All trace element profiles were first detrended using a LOESS filter with a span of

293   0.2 times the length of the record to remove longer term (i.e., seasonal to multi-annual) trends.

294   The detrended series were linearly resampled in the time domain before applying the Multi-Taper

295   Method (MTM; (Thomson, 1982)) to extract dominant frequencies from the data. Spectral analysis

296   was carried out using the "astrochron" package (Meyers, 2014) in R ((R Core Team, 2013); see

297   script in **S6**). The significance of relevant periodicities was tested using a combination of "red

298   noise" estimation and a harmonic F-test (see (Meyers, 2012)). To visualize the evolution of

299   periodic behavior across the shells, wavelet analysis was applied on all trace element profiles

300   using the "dplR" package in R (see **S6**).

301

302   2.7 Extracting high-resolution variability

303   After detrending and spectral analysis, all trace element profiles were smoothed using a Savitzky-

304   Golay filter with a width of 21 datapoints (8.4 µm; equivalent to a timespan of ~1-5 h; **S6**) to

305   remove high-frequency measurement noise within our LA-ICP-MS spot size. The Savitzky-Golay

306   filter was used because it preserves the tendency of the trace element profile and therefore retains

307   a larger fraction of the amplitude of periodicity close to the width of the filter compared to simpler

308   smoothing techniques (e.g. moving average; (Savitzky and Golay, 1964)). The 21-point window

309   size was chosen to smooth out the maximum amount of instrumental noise without losing

310   periodicity larger than half the width of the laser spot (0.22 µm; equivalent to 23 datapoints).

311   Statistically significant (see **section 2.6**) variability in daily (~22-36 h; centered on the 24 h diurnal

312   cycle) and semi-diurnal (~8-14 h; centered on the 12.4 h tidal cycle) frequency bands was

313   extracted from the trace element records using a combination of bandpass filtering (using the

314   "bandpass" function in the "astrochron" R package) and stacking (see **S6**). Trace element data

315   was stacked along bandpass filters using the following procedure: Maxima and minima in the

316   bandpass filter were used as tie points to reference each datapoint of the smoothed dataset

317   relative to its position within the cycle on a scale from 0 to 1. These relative positions were then

318   used to divide the data into 10 bins (bin 1 contains positions 0 – 0.1, bin 2 contains data from

319   positions 0.1 – 0.2, etc.), providing stacked data a resolution of 0.1 times the length of the cycle

320   under investigation. The full breakdown of variability within and between bins created in the

321   stacking routine is provided in **S7**. Different sources of variance in the trace element records were

322   isolated by sequentially determining the variance left in the trace element records after each of

323   the data treatment steps explained above (see example in **S7**). This procedure allowed us to

324   quantify the amount of variance in each trace element profile explained by either diurnal or semi-

325   diurnal variability.

3. Results

3.1 Trace element data

LA-ICP-MS line scans yielded profiles of Sr/Ca, Mg/Ca, Mn/Ca and Ba/Ca in growth direction on 11 cross-sections through shells of *P. maximus*, *T. maxima*, *T. squamosa* and *T. squamosina* (**Fig. 2**; see **S0** for raw data of all scans). Sub-millimeter scale patterns in Sr/Ca, Mg/Ca, Mn/Ca, and Ba/Ca are highly reproducible between consecutive line scans on the same LA-ICP-MS transect: R^2 values typically exceed 0.8, and mean element ratio differences between time equivalent samples in different line scans are typically <0.05 mmol/mol for Mg/Ca (<5 % relative to mean value), <0.02 mmol/mol for Sr/Ca (<2 % relative to mean value), <0.5 µmol/mol for Mn/Ca (<10 % relative to mean value) and <0.2 µmol/mol for Ba/Ca (<8 % relative to mean value; see **S2**). Remeasured transects further away from the outer shell surface in tridacnids (see **section 2.4**) differ more from the original transects than those measured on the exact same locality in the shell: R^2 values between parallel lines in different localities are 0.3 – 0.5 for Mg/Ca and Sr/Ca and <0.3 for Mn/Ca and Ba/Ca, reflecting intra-shell variability in trace element composition in the tridacnids (**S2**). Overall, sub-millimeter scale patterns in trace element composition are reproduced in parallel line scans. Finally, "rib" and "valley" segments through the same specimen of *P. maximus* show similar patterns in trace elements, but element-to-calcium ratios (especially Ba/Ca and Mn/Ca) can be quite different, highlighting heterogeneity within the shells of *P. maximus* (**Fig. 2**).

Trace element profiles in pectinids, reflecting only one growing season, show Sr/Ca and Mg/Ca maxima in the middle of the profile, while Mn/Ca and Ba/Ca are more variable, showing multiple peaks in the same growth year. Peaks in Mn/Ca and Ba/Ca are synchronous between profiles through the same specimen, but not between specimens. Tridacnid Mg/Ca, and Sr/Ca ratios show one or two distinct cycles per growth year. Mn/Ca and Ba/Ca ratios in tridacnids show more regular annual or biannual variability than pectinids (most notably specimen **SQSA1**). It must be

351   noted, however, that *P. maximus* shells only recorded one growth season, limiting the

352   interpretation of seasonal growth patterns.

353   Plots of trace element variability zoomed in on smaller sections of the record reveal dominant

354   high-frequency variability superimposed on seasonal-scale patterns (**Figure 3**). Both tridacnid

355   and pectinid LA-ICP-MS records show distinct high-frequency cyclicity in all studied trace

356   element-to-Ca ratios with amplitudes on nearly the same order of magnitude as the longer-term

357   variability described by the records on a seasonal to multi-annual scale (**Fig. 2**).

358
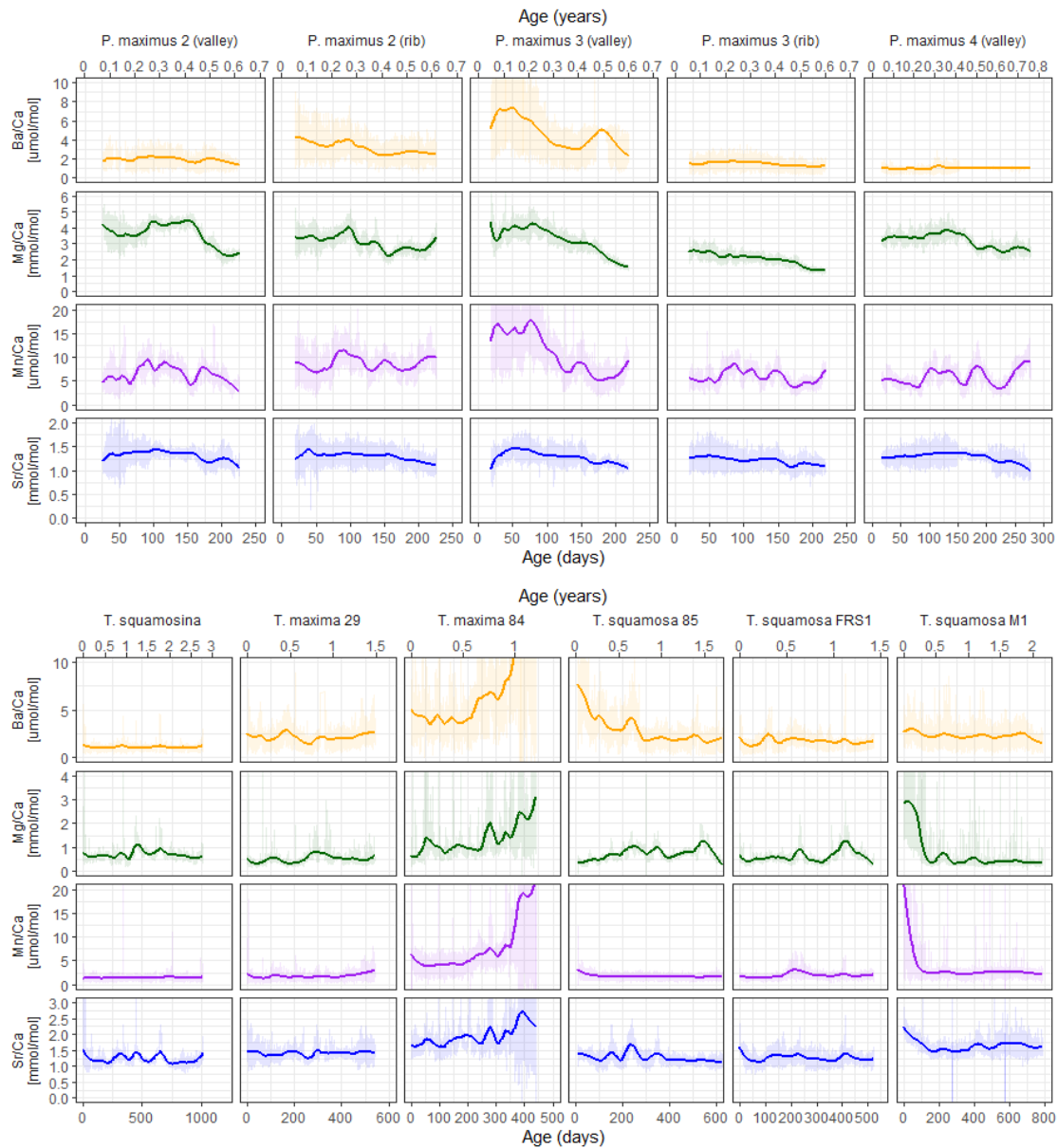
Figure **2**: Overview of LA-ICP-MS results of Sr/Ca (blue), Mg/Ca (green), Mn/Ca (purple) and Ba/Ca (orange) in pectinid (upper panel) and tridacnid (lower panel**)** specimens. Vertical axes are equal for plots positioned next to each other (but different for the two groups of tridacnid and pectinid plots). Shaded lines show raw LA-ICP-MS data while solid lines indicate 0.2 span LOESS fits through the data highlighting monthly-scale variability. A direct comparison of trace elemental ratios between specimens is provided in **S8**.
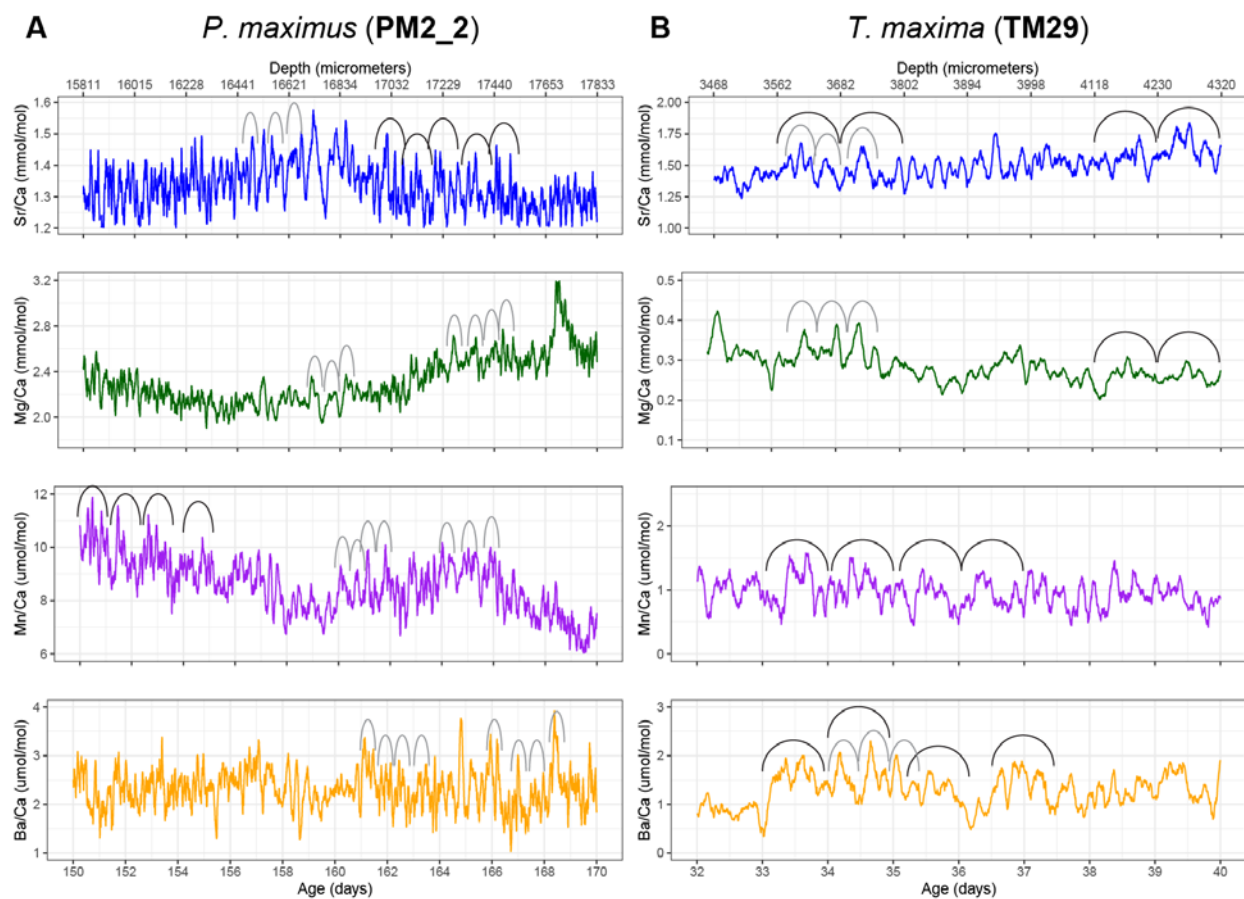
Figure 3: Plots showing samples of semi-diurnal and daily variability in Savitzky-Golay filtered trace element ratios in selected intervals through *P. maximus* specimen **PM2_2** (**A**; 51-point filter) and *T. maxima* specimen **TM29** (**B**; 21-point filter). Filters isolate hour to daily scale variability while filtering out the higher-order measurement noise. Arches indicate examples of the expression of daily (black) and semi-diurnal (grey) cycles in the records.

371

3.2 Age models

Growth line counting in the *P. maximus* shells was repeated multiple times on both the outer shell surface and in cross sections through the shell by different persons (**Table 1**; **S3**). The variability in counting results shows that the growth lines were not always equally easy to distinguish. In **PM2** and **PM3**, the most likely number of increments (228 and 220 respectively) was confirmed in both cross sections and on the outside of the shell. In **PM4**, counting in the cross section (278 increments) was chosen over the slightly lower count on the outside of the shell (272-273 increments) since the LA-ICP-MS profile was measured on the same cross section and could be directly linked to the counted increments. Note that, while the consistency in daily counts between specimens from the same year and environment is encouraging, inter-specimen variability in the onset of spring growth or the onset of the winter stop (potentially prior to the collection date of November 15th, 2019) places some uncertainty on the absolute date assigned to *P. maximus* shell sections (Chauvaud et al., 2005). The age-distance relationships (growth curves) resulting from the sclerochronology are shown in **S5**.

386

387 **Table 1: Growth increments counting in *P. maximus***

Specimen	Increments counted on outer surface	Increments counted in cross sections	Mean daily increment width [µm ± 1σ]
PM2	226, **228**, 234, 241	227, **228**, 233	249 ± 19
PM3	**220**, 226, 243	213, **220**, **220**	249 ± 22
PM4	272, 273	**278**	247 ± 4

388

389

390   Layer counting in tridacnid shells yielded estimates of semi-diurnal, daily and annual growth

391   (**Table 2**; **S4**). Annual growth rates calculated from layer counting are highly consistent between

392   specimens from the same species from the same environment (within 1 mm/yr; **Table 2**), lending

393   confidence to the growth line counting results. The von Bertalanffy growth models based on these

394   growth line counts are plotted in **S5**. Statistics of the parameters (L_{inf} and k) of these growth

395   models and their uncertainty are provided in **S4**.

396

397   **Table 2: Growth line counting in *Tridacna* shells.** Column 3 shows the total number of

398   increments counted in the specimen, column 4 shows their median width and column 5 shows

399   the width of an annual increment in the specimen. Note that increments could not be counted over

400   the entire growth period of the shells, so the numbers in column 3 represent representative

401   numbers of increments counted in those parts of the shells where they were distinct enough for

402   counting (see **section 2.5**). Increment timing (semi-diurnal vs diurnal) was established based on

403   the relative difference between increment width and the distance between annual growth breaks

404   measured on the outside of the shells.

Specimen	Species	# counted increments	Median increment width [µm]	Annual growth [mm]	Increment timing
TM29	*T. maxima*	274	26.5	27.9	Semi-diurnal
TM84	*T. maxima*	109	39.1	26.6	Diurnal
TS85	*T. squamosa*	310	40.3	20.2	Diurnal
TSFRS1	*T. squamosa*	225	23.3	20.1	Semi-diurnal
TSM1	*T. squamosa*	180	33.3	20.6	Diurnal
SQSA1	*T. squamosina*	153	22.3	14.9	Diurnal

405

406

407   3.3 Growth rates and temporal sampling resolution

408   Growth rates are highly similar between specimens of the same species (**Table 1 and Table 2**;

409   **S3-5**), with *P. maximus* achieving the highest growth rates (~ 220 growth days * ~ 250 µm/d ≈ 55

410   mm/yr; **Table 1**), followed by *T. maxima* (~27 mm/yr; **Table 2**), *T. squamosa* (~20 mm/yr; **Table**

411   **2**) and *T. squamosina* (15 mm/yr; **Table 2**). Dividing the width of the daily increments (e.g., 250

412   µm for *P. maximus*) by spatial LA-ICP-MS sampling resolution of 0.44 µm (see **section 2.4**), these

413   growth rates would seem to translate to a temporal resolution of 0.04 h, 0.24 h, 0.44 h and 0.27

414   h for *P. maximus*, *T. maxima*, *T. squamosa* and *T. squamosina*, respectively. However, our LA-

415   ICP-MS spot size (20 µm in sampling direction) causes significant smoothing, reducing the

416   frequency that can be resolved. Nevertheless, our test applying the LA-ICP-MS settings on a

417   virtual Sr/Ca dataset with the characteristics of the diurnal record by (Sano et al., 2012) and

418   growth rates equivalent to our specimens (see **S13**) reveals that our analytical methodology can

419   easily resolve daily variability even in our slowest-growing specimen (*T. squamosina* **SQSA1**),

420   conserving at least 75 % of the signal amplitude. The LA-ICP-MS profiles record trace element

421   variability during growth periods ranging between 220 days (for **PM3**) and 1041 days (for **SQSA1**).

422

423   3.4 Spectral analysis

424   Normalized power spectra and significance level of daily and tidal periodicities in pectinid and

425   tridacnid records are shown in **Figure 4** and **Figure 5**, respectively. Full spectral analysis results

426   for all trace element records in all specimens are provided in **S9**. All *P. maximus* power spectra

427   (**Fig. 4**) reveal semi-diurnal (12 h) periodicity in Sr/Ca and Ba/Ca with > 86 % statistical

428   significance. Only sections through the ribs of the shells (**PM2_1** and **PM3_1**) show semi-diurnal

429   periodicity in Mg/Ca and Mn/Ca (> 90 % significance). Daily periodicity is present in some, but not

430   all, pectinid profiles. Most pectinid trace element records also contain multi-day periodicities,

431   including strong 7-day periodicities and weaker cyclicity associated with 14-day and 28-day

432   cycles. The latter is partly suppressed by the 0.2 span LOESS filter (equivalent to a 44-56 day

433   period depending on the length of the record) applied on the records to remove the seasonal trend

434   from the records. However, these lower frequency cycles are clearly visible in the wavelets (see

435   **S9**).

436   Tridacnid trace element profiles show more consistent daily periodicity than pectinid records (**Fig.**

437   **5**). Especially Sr/Ca and Ba/Ca records through nearly all tridacnid specimens exhibit strong (>

438   90 % confidence level) power in the daily period, while daily cyclicity is weaker in Mn/Ca and

439   Mg/Ca records. Sr/Ca records in the tridacnids also contain a significant (> 96 %) semi-diurnal

440   component, whose tidal origin seems clear in most specimens by peaks in power in the longer (7

441   d, 14 d and 28 d) tidal components.
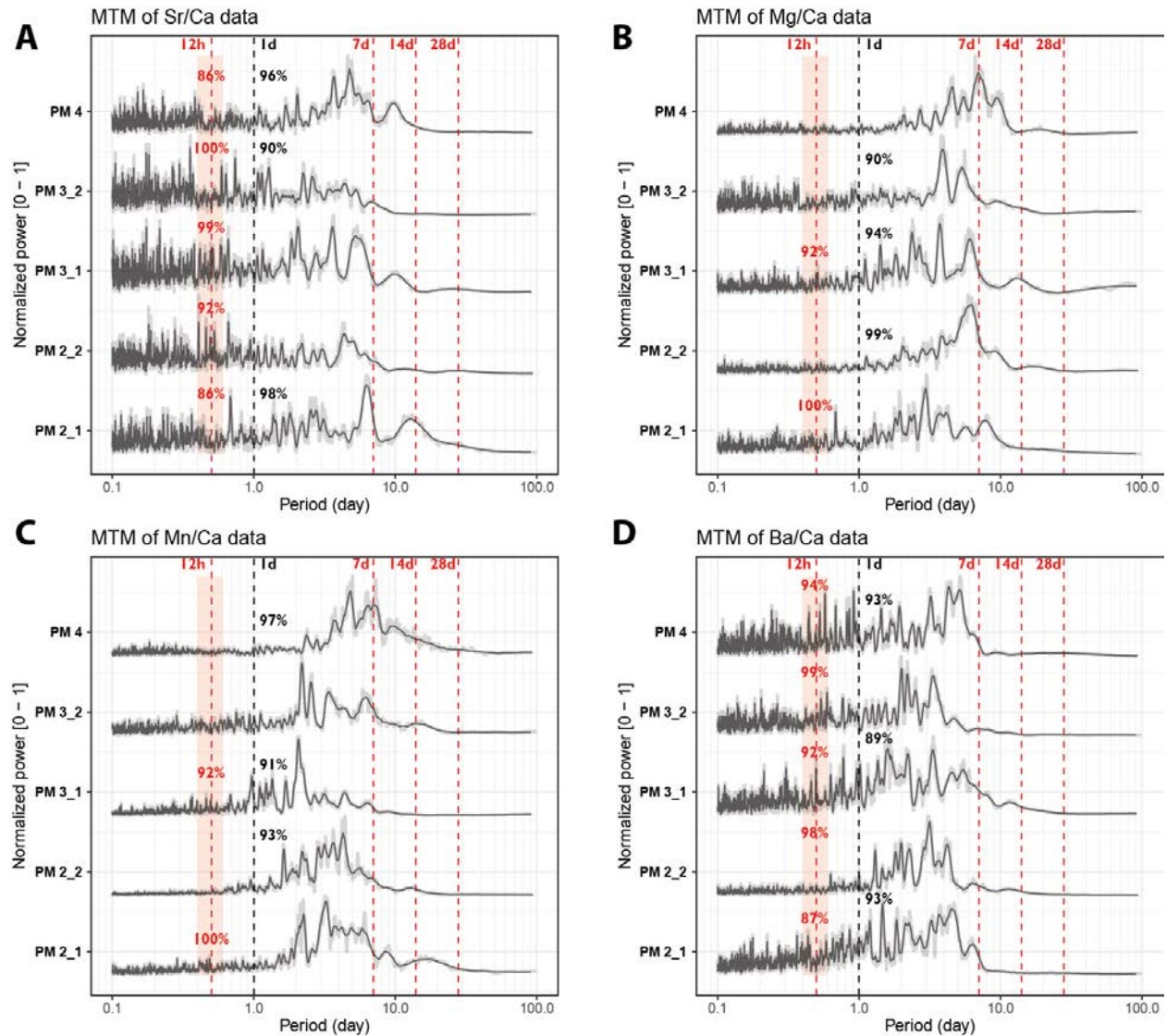
Figure 4: Multi-taper method spectrograms of Sr/Ca (**A**), Mg/Ca (**B**), Mn/Ca (**C**) and Ba/Ca (**D**) records through the five pectinid cross sections after detrending (see **section 2.6**). All spectra are normalized by dividing by the highest power peak and plotted on the same horizontal axis. Grey shaded lines show raw data while solid black lines plot 21-point moving average smoothed curves. Red vertical dashed lines highlight the expected periods of tidal variability while black vertical dashed lines indicate 1-day periodicities. Significance levels of peaks on these periods (see **section 2.6** and (Meyers, 2012)) are rounded to the nearest whole percentage point.

450
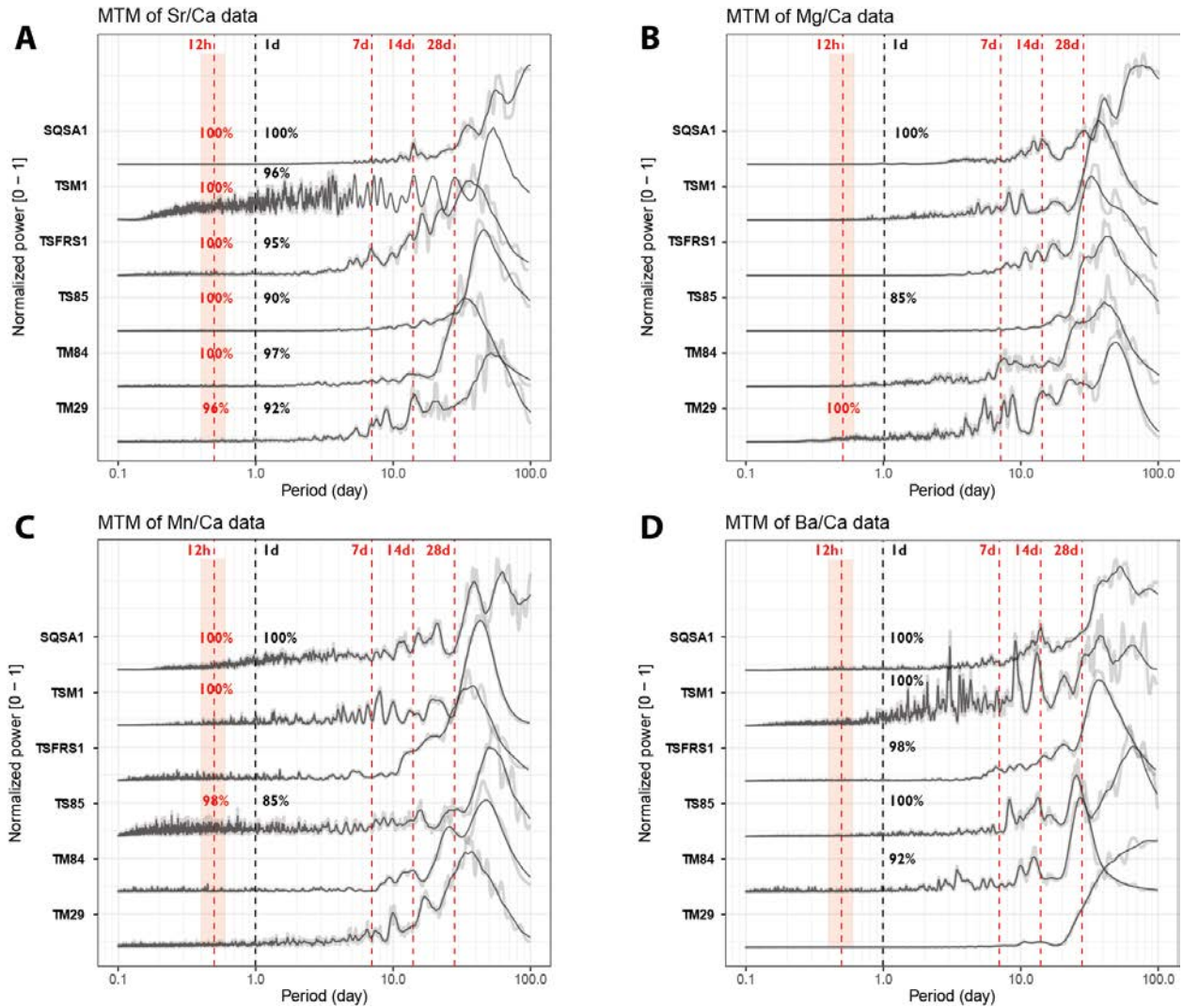
Figure 5: Multi-taper method spectrograms of Sr/Ca (**A**), Mg/Ca (**B**), Mn/Ca (**C**) and Ba/Ca (**D**)

records through the six tridacnid cross sections after detrending (see **section 2.6**). All spectra are

normalized by dividing by the highest power peak and plotted on the same horizontal axis. Grey

shaded lines show raw data while solid black lines plot 21-point moving average smoothed

curves. Red vertical dashed lines highlight the expected periods of tidal variability while black

vertical dashed lines indicate 1-day periodicities. Significance levels of peaks on these periods

(see **section 2.6** and (Meyers, 2012)) are rounded to the nearest whole percentage point.

458

459 3.5 Variance decomposition

460 Variability at the daily (24 h) and semi-diurnal (12 h) scale in all trace element records through all

461 specimens was extracted using bandpass filtering (**section 2.7;** see **S9** and **S10**). The median

462 amplitude of variability within these stacks was plotted against the median period of the variability

463 per element and per specimen to highlight dominant periodicities in the trace element data

464 (**Figure 6**). As noted in the spectral analysis results (**section 3.4**), trace element composition in

465 tridacnid shells is more strongly controlled by daily variability than in pectinid shells (**Fig. 6**; **S10**).

466 The difference is especially noticeable in Sr/Ca and Ba/Ca ratios, which show a clear divide

467 between daily periodicity in tridacnid shells and tidal periodicity in pectinids (see **Fig. 6**). The

468 differences in Mg/Ca and Mn/Ca ratios are less obvious.

469

470
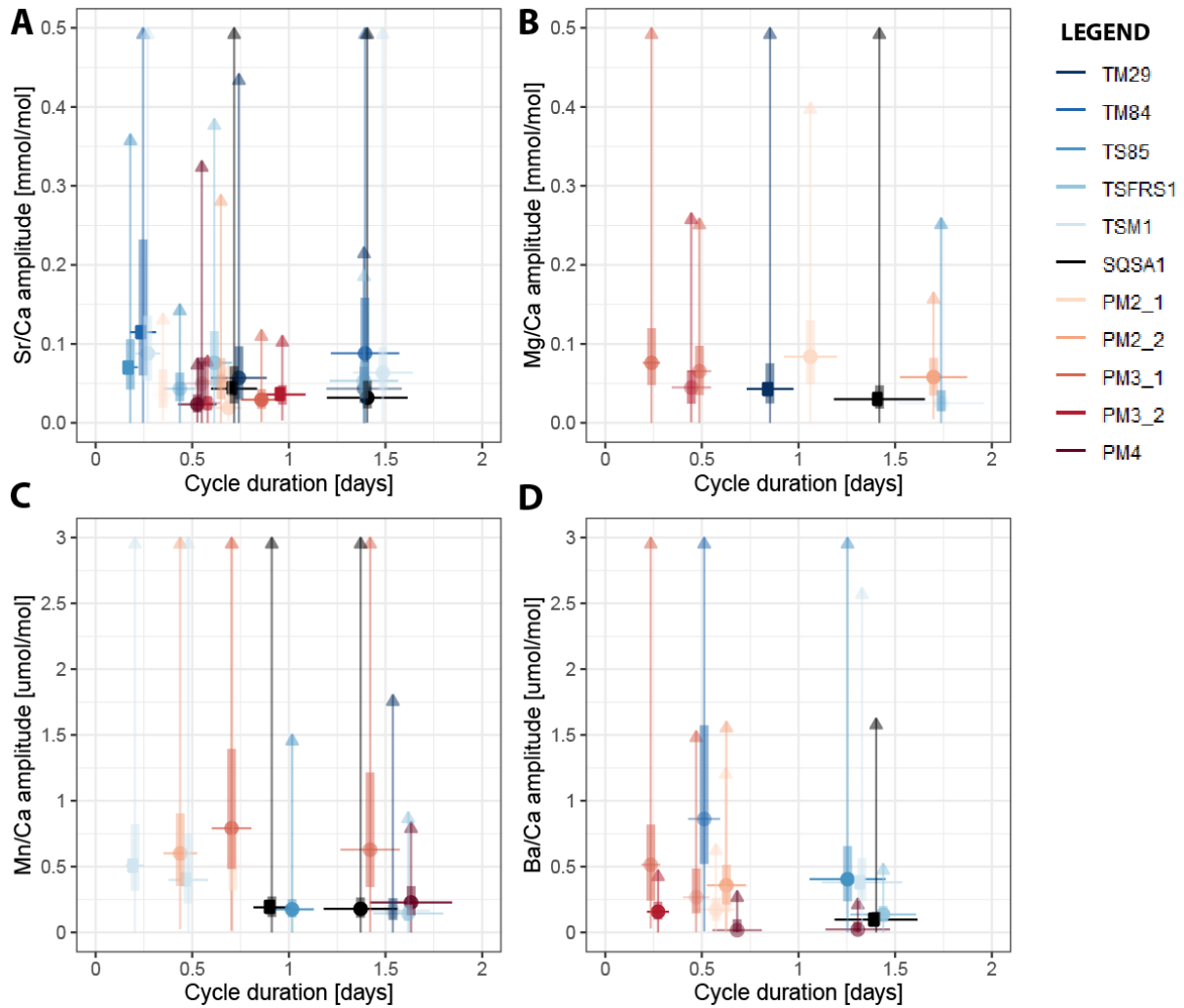
Figure 6: Cross plot showing the amplitude of variability of dominant spectral periods in Sr/Ca (**A**), Mg/Ca (**B**), Mn/Ca (**C**) and Ba/Ca (**D**) against the period (duration) of the cycle. Round symbols indicate the median amplitude of the cycle, while vertical bars and lines show interquartile differences and ranges in the amplitude over the record. Horizontal bars indicate the width of the bandpass filter used to extract periodic variability. Colors highlight different specimens (see legend).

477

478   An example of the distribution of normalized variability within the trace element records after each

479   data processing step is shown in **S7**. This example shows that a large fraction of the variance in

480   the records (73 % in this record after trimming outliers) is explained by low-frequency (seasonal

481   scale) variability (**S7**). Of the remaining smoothed and detrended dataset, at most 20 % of the

482   variance is explained by daily and tidal (semi-diurnal) periodicity (see **Figure 7** and **Table 3**). A

483   full decomposition of variance in all trace element records through all specimens is provided in

484   **S7**. **Figure 6** and **Figure 7A** show that, overall, the variance explained by daily periodicity is

485   higher in tridacnids than in pectinids (Wilcoxon signed rank test; W = 44; p = 0.009). The difference

486   between species is smaller for tidal variability (**Fig. 7B**). There is no clear difference in relative

487   dominance of semi-diurnal variability between trace element records, but daily variability is more

488   strongly expressed in Ba/Ca and Mn/Ca records, especially in tridacnid shells. Finally, *T.*

489   *squamosa* specimen **TSM1**, which grew under a sunshade, does not exhibit significantly lower

490   daily periodicity compared to the other tridacnid specimens.

491

492
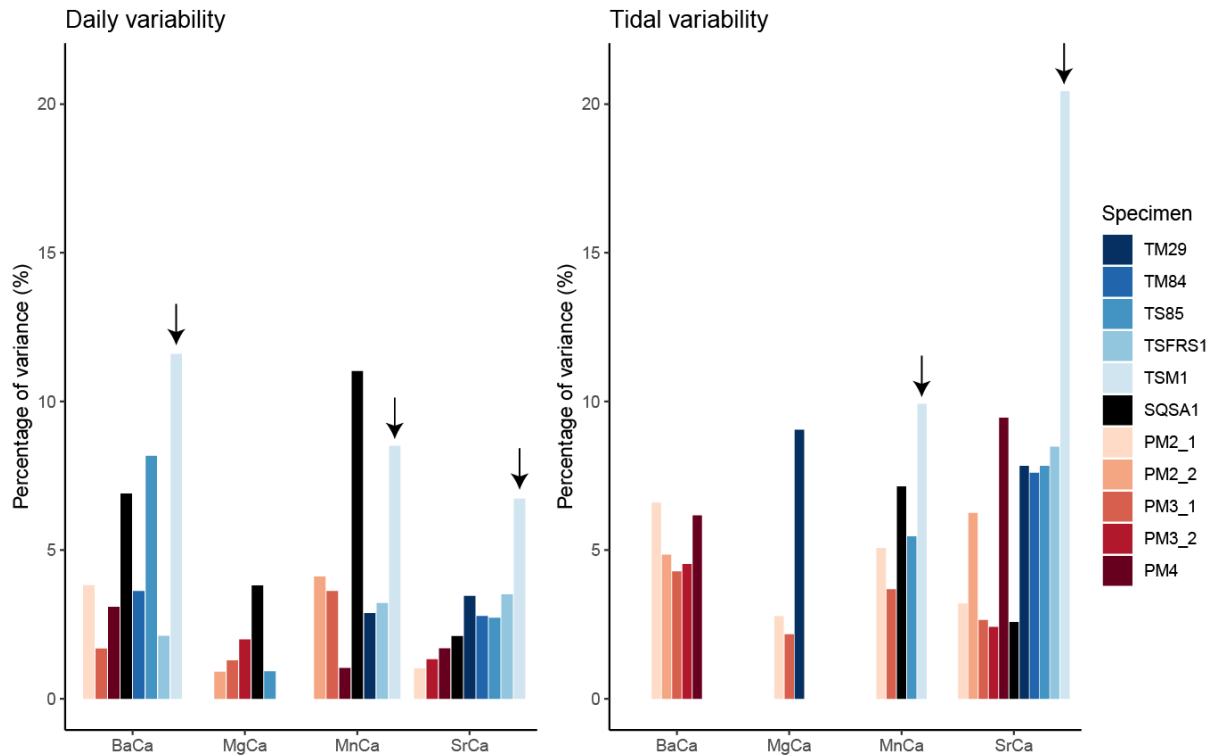
Figure 7: Summary of relative variance (in %) of significant daily (left) and tidal (right) variability

extracted from trace element records. Colors highlight different specimens (see legend). Note that

the *T. squamosa* specimen **TSM1** which grew under a sunshade is highlighted with a black arrow.

496

497 **Table 3**: Overview of the relative (in %) variance associated with daily and tidal variability in all
498 trace element records through all specimens. Empty cells represent records for which no
499 significant tidal or daily periodicity was found (see **Fig. 4-5**).

	Daily variance [% relative to detrended record]				Tidal variance [% relative to detrended record]			
	Ba/Ca	Mg/Ca	Mn/Ca	Sr/Ca	Ba/Ca	Mg/Ca	Mn/Ca	Sr/Ca
PM2_1	3.8 %			1.0 %	6.6 %	2.8 %	5.1 %	3.2 %
PM2_2		0.9 %	4.1 %		4.9 %			6.3 %
PM3_1	1.7 %	1.3 %	3.6 %		4.3 %	2.2 %	3.7 %	2.7 %
PM3_2		2.0 %		1.3 %	4.5 %			2.4 %
PM4	3.1 %		1.0 %	1.7 %	6.2 %			9.5 %
TM29			2.9 %	3.5 %		9.0 %		7.8 %
TM84	3.6 %			2.8 %				7.6 %
TS85	8.1 %	0.9 %		2.7 %			5.5 %	7.8 %
TSFRS1	2.1 %		3.2 %	3.5 %				8.5 %
TSM1	12 %		8.5 %	6.7 %			10 %	20 %
SQSA1	6.9 %	3.8 %	11 %	2.1 %			7.1 %	2.6 %

500

501
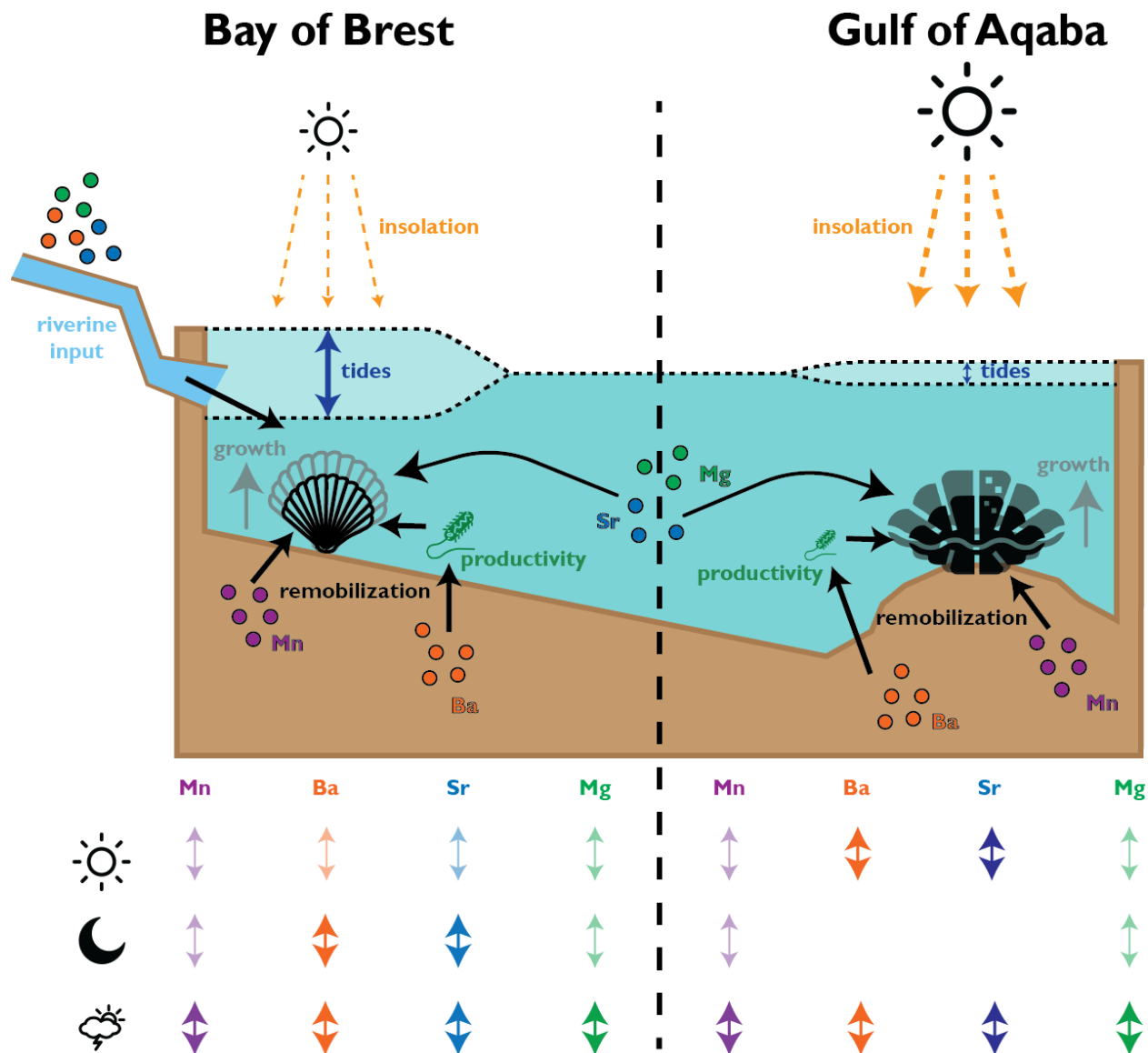
Figure 8: Schematic overview of environmental parameters interpreted to affect shell growth and composition of pectinids in the Bay of Brest and tridacnids in the Gulf of Aqaba. The table at the bottom provides a schematic qualitative overview of the amount of variance in the trace element records of the taxa is explained by daily (sun symbol), tidal (moon symbol) or aperiodic (cloud symbol) variability in the environment.

507

4. Discussion

4.1 Compositional differences between pectinids and tridacnids

Pectinid and tridacnid shells are characterized by similar mean Sr/Ca and Ba/Ca ratios (Sr/Ca of 1.3 ± 0.3 and 1.5 ± 0.6 mmol/mol respectively; Ba/Ca of 2.8 ± 2.5 and 3.0 ± 5.1 µmol/mol respectively; uncertainty is calculated as 1 σ). Mean Mg/Ca and Mn/Ca ratios are higher in *P. maximus* than in *Tridacna* species (Mg/Ca = 3.1 ± 0.9 and 0.7 ± 0.9 mmol/mol; Mn/Ca = 7.8 ± 4.7 and 2.7 ± 7.8 µmol/mol; 1 σ; **Figure 2**; **S4**). The incorporation of higher concentrations of the elements Mg and Mn, which have a lower ionic radius than Sr and Ba, in calcitic pectinid shells compared to aragonitic tridacnid shells makes sense given the higher partition coefficient of these elements in calcite than in aragonite (Day and Henderson, 2013; Wassenburg et al., 2016).

Differences between tridacnid specimens generally exceed the differences between tridacnids and pectinids (1σ of Ba/Ca among all tridacnid specimens = 2.1 µmol/mol), suggesting large inter-species differences. However, individual records such as those in **TM84** and **PM3_1** show large variability (especially in Ba/Ca and Mn/Ca) compared to other specimens of the same species. Inter-specimen variability is higher in tridacnid shells than in pectinids (inter-specimen relative standard deviations as a fraction of mean ratio for Ba/Ca: 0.74 vs 0.64 µmol/mol, Mg/Ca: 0.37 vs 0.20 mmol/mol, Sr/Ca: 0.19 vs 0.03 mmol/mol and Mn/Ca: 0.78 vs 0.33 µmol/mol for tridacnids and pectinids, respectively). **Figure 2** shows that this variability between tridacnids is not readily explained by differences between species, but mostly reflects differences in the trends within the records, with some specimens (e.g., **TM84**, **TSM1** and **TS85**) showing trends in composition towards the end of the record (see also **S8**). It thus seems that inter-specimen differences, perhaps driven by growth stress, are dominant drivers of trace element variability in giant clams. This interpretation is corroborated by the observation that trace element compositions in tridacnid shells are significantly more skewed towards higher values than in pectinids (mean skewness per element and per specimen is 9.7 for tridacnids and 0.9 for pectinids). This skewness reflects the

533 high peaks in trace element composition observed in tridacnid profiles, especially near the ventral

534 margin (e.g., specimens **TM84**, **TSM1** and **TS85**; see **section 2.4**; **Fig. 2**; **S8**), which hint towards

535 growth disturbances at the individual level.

536 4.2 Trace element variability in *P. maximus*

537 4.2.1 Comparison with previous studies

538 Trace element concentrations in *P. maximus* analyzed in this study are in close agreement with

539 concentrations found in wild (live collected) pectinid shells in the literature (Lorrain et al., 2005;

540 Barats et al., 2008; Poitevin et al., 2020; Fröhlich et al., 2022). In these studies, Sr/Ca shows a

541 strong link with calcification rate (as measured by the width of daily shell increments; (Lorrain et

542 al., 2005)), although previous studies did not assess variability on the (sub-)daily scale. The long-

543 term trends in our Sr/Ca records seem to confirm this correlation, with higher values being

544 recorded in the middle of the growing season (day 50-150; **Fig. 2**) when growth rates are highest

545 (see **S5**). Previous studies demonstrate that Mg/Ca ratios in pectinid shells are at most

546 partially related to temperature and/or salinity (Lorrain et al., 2005; Poitevin et al., 2020).

547 The fact that the studied *P. maximus* specimens, which all grew during the same year in the

548 same environment, do not show a synchronous Mg/Ca pattern (**Fig. 2**) corroborates this

549 previous work and argues against a straightforward temperature dependence for Mg/Ca in *P.*

550 *maximus*. In addition, the lack of strict coherence between profiles of Mg/Ca (and other elements)

551 in parallel transects through *P. maximus* shells (e.g., **PM2_1** and **PM2_2**; **Fig. 2**) hints at

552 compositional heterogeneity within the shells, in agreement with findings by (Lorrain et al.,

553 2005). Low correlations between profiles through the same shell at the daily scale are also partly

554 driven by small misalignments of the timing of shell formation between the transects at the sub-

555 millimeter scale and variations in the height of trace element peaks, especially in Mn/Ca and

556 Ba/Ca, which are higher further towards the outside of the shell (**S2**).

557   There is evidence suggesting that Mg content varies in mollusk shells in function of the amount

558   of organic matter in the biomineral (Dauphin et al., 2003; Richard, 2009; Tanaka et al., 2019).

559   Contrarily, Mn is known to be taken up in thermodynamic equilibrium in the mineral fraction of

560   bivalve shells (Onuma et al., 1979; Soldati et al., 2016), and Mn/Ca ratios in *P. maximus* have

561   been shown to faithfully record fluctuations of dissolved Mn in the coastal environment driven by

562   riverine input and redox conditions (Barats et al., 2008). Similarly, there is strong evidence that

563   Ba/Ca ratios in *P. maximus* (and other mollusks) record changes in Ba available in the

564   environment linked to primary productivity (e.g., (Gillikin et al., 2008; Thébault et al., 2009;

565   Fröhlich et al., 2022). Interestingly, our results (Fig. 2) show that background Ba/Ca values are

566   not equal in the shells of *P. maximus* and tridacnid specimens grown in the same environment.

567   This contradicts the assessment by (Gillikin et al., 2005) that background Ba/Ca concentrations

568   are a function of environmental conditions and can be consistently subtracted from Ba/Ca records

569   to separate peak from background values. The suggested relationship between Ba/Ca and

570   primary productivity would explain the skewed (skewness > 1; **S8**) character of the Ba/Ca records

571   and the correlation between Ba/Ca and Mn/Ca in the studied *P. maximus* specimens, as the

572   reducing conditions following peaks in primary productivity favor the remobilization of Mn into the

573   water column causing short-lived simultaneous increases in Ba/Ca and Mn/Ca in the shells

574   (Dehairs et al., 1989; Barats et al., 2008, 2009).

575   4.2.2 Short-term changes in shell composition in *P. maximus*

576   In the context of the high-resolution trace element variability central to this study, it seems

577   plausible that short-term changes in the environment of the Bay of Brest were drivers of Mn/Ca

578   and Ba/Ca variability in *P. maximus* shells, while Mg/Ca and Sr/Ca composition is mostly driven

579   by changes in calcification rate. This would suggest that the significant tidal (12 h) component in

580   Ba/Ca and Mn/Ca records through *P. maximus* (**Fig. 4**) is driven directly by redox changes over

581   the strong tidal cycle in the Bay of Brest (see (Polsenaere et al., 2021)) and resuspension of Ba

582   and Mn due to tidal currents (Hily et al., 1992), while tidal rhythms in Mg/Ca and Sr/Ca may be a

583   consequence of the scallop's calcification response to changes in its environment (e.g.,

584   temperature, salinity and light availability) through the large (up to 7 m range) tidal cycle (**Fig. 8**).

585   The latter corroborates with previous studies in other calcitic mollusk shells which demonstrated

586   that Mg incorporation on short timescales is driven by the metabolic response to subtle changes

587   in the environment (Lazareth et al., 2007). Finally, care must be taken to interpret trace element

588   variability in *P. maximus* shells, since large intra-shell gradients in Mg/Ca, Sr/Ca and Mn/Ca have

589   previously been observed in this species, making trace element composition highly dependent on

590   the location of measurements relative to the outer shell surface or positioning relative to striae on

591   the shell surface (Freitas et al., 2009). Even though the LA-ICP-MS line scans in this study

592   targeted exclusively the oOSL of *P. maximus* specimens, variability in elemental ratios resulting

593   from small changes in the distance of the line scan from the outer edge of the shell cannot be fully

594   excluded (Richard, 2009).

595

596   4.3 Trace element variability in tridacnids

597   4.3.1 Comparison with previous studies

598   Results for Sr/Ca, Mg/Ca and Ba/Ca in this study's tridacnid specimens broadly corroborate trace

599   element results in other tridacnid studies (e.g., (Elliot et al., 2009; Sano et al., 2012; Yan et al.,

600   2013; Warter et al., 2018)). While data on Mn/Ca in the OSL of tridacnids is scarce, the Mn/Ca

601   ratios in tridacnids in this study (mean Mn/Ca = 7.8 ± 4.7 µmol/mol) are similar to LA-ICP-MS

602   Mn/Ca data available in the literature ((Warter et al., 2015), 4-10 µmol/mol), but significantly lower

603   than Mn/Ca values measured using total digestion Atomic Absorption Spectrometry ((Madkour,

604   2005), ~30 µmol/mol). The main difference between the techniques is that LA-ICP-MS (both in

605   this study as in (Warter et al., 2015)) sampled shell layers where growth lines were visible and

606   did not include pre-treatment, while the total digestion study (Madkour, 2005) removed organic

607   matter by roasting the shells at 200°C prior to bulk shell analysis. Given that Mn in bivalve shells

608   is typically associated with the mineral fraction of the shell (Soldati et al., 2016), the difference in

609   results may therefore hint at differences between shell layers within tridacnids, or differences in

610   Mn concentration between the organic and mineral fractions in the shells. Bivalve shells typically

611   contain between 1 % and 5 % organic matter (Marin and Luquet, 2004), with tridacnid shells being

612   notable for their low organic matter content (< 1 %; (Taylor and Layman, 1972; Agbaje et al.,

613   2017))., It thus seems unlikely that the differences in Mn/Ca ratio between bulk analyses

614   (Madkour, 2005) and *in situ* analysis ((Warter et al., 2015); this study) could originate from

615   variations within the organic matrix, which only constitutes such a small fraction of the shell.

616   Therefore, we consider a difference in Mn concentration between shell layers in tridacnids more

617   likely. The lack of consistent trace element offsets between the tridacnid species under study here

618   (*T. maxima*, *T. squamosa* and *T. squamosina*) confirms the chemical similarities of shells tridacnid

619   species found in previous studies (e.g., *T. gigas*; (Elliot et al., 2009; Yan et al., 2013); *T. crocea*;

620   (Warter et al., 2018); *T. derasa*; (Sano et al., 2012)).

621   4.3.2 Short-term variability in Sr/Ca paced to the day-night cycle

622   Sr/Ca in tridacnids is hypothesized to be strongly controlled by light intensity through a circadian

623   rhythm linked to the day-night cycle (Sano et al., 2012; Warter et al., 2018). This would explain

624   the strong daily periodicity in Sr/Ca records through all tridacnids in this study. This daily

625   periodicity may be caused by the ctenidium in tridacnids working on a daily rhythm to keep the

626   acid-base balance in the hemolymph of the clams to offset the CO_2 depletion by photosymbionts

627   (which is paced to the day-night cycle of light availability). In the process, Ca^{2+}-channels and

628   Na^+/H^+-exchangers work to keep the charge balance in the internal fluid and provide nutrients and

629   ions for shell mineralization, letting in compatible trace elements such as Sr^{2+} (Ip and Chew,

630   2021). This mechanism follows the biomineralization model by (Carré et al., 2006) and is

631   supported by the high affinity of Sr^{2+} with Ca-channels (Hagiwara and Byerly, 1981) and the high

632   ionic fluxes supported by this pathway, allowing enough membrane permeability to support the

633   fast shell formation in tridacnids (Coimbra et al., 1988; Sather and McCleskey, 2003). Following

634   this line of reasoning, the preconcentration of Sr^{2+} in the extrapallial fluid through Ca-channels

635   should have a larger effect on shell Sr/Ca ratios in tridacnids than the discrimination against Sr^{2+}

636   (or other trace elements) through shell organic matrix during mineralization of the shell from this

637   fluid (as proposed in (Gillikin et al., 2005)). This model could explain the indirect link between

638   trace element incorporation into the shell of tridacnids and the day-night cycle without a direct

639   causal relationship between trace element concentration and light availability (as demonstrated

640   by the strong daily cycle in trace elements in the shaded **TSM1** specimen). It is worth noting that

641   experiments on freshwater bivalves (e.g., *Corbicula fluminea*; (Zhao et al., 2017)) revealed that a

642   closure of the Ca^{2+} channels did not influence Sr concentrations in the shell, arguing against a

643   kinetic effect on Sr partitioning into the shell.

644   4.3.3 Tidal vs. diurnal variability

645   Our spectral analysis does not allow us to distinguish between the expression of the solar day (24

646   h) and lunar day (~24.8 h) because the width of the bandpass filters used to extract periodicities

647   (~22–36 h) encompass both frequencies. While we cannot exclude the possibility that some of

648   the daily (24 h frequency band) periodicity in tridacnid records is an expression of the lunar cycle,

649   it seems unlikely for most records except Sr/Ca, because the expression of the other lunar

650   periodicities (most notably the ~12 h cycle) is much weaker in tridacnids compared to the pectinids

651   (see **Fig. 6-7**). Nevertheless, it remains possible that the diurnal cycle in Sr/Ca in tridacnids,

652   previously interpreted as a response to the day-night cycle, is in fact caused by a circadian rhythm

653   paced to the lunar day. Additionally, vertical mixing, a major driver of sea surface temperature

654   changes in the northern Gulf of Aqaba, is shown to be driven by a combination of surface wind

655   intensity (which has strong daily variability) and the presence of tidal currents (Carlson et al.,

656   2014). It is therefore possible that changes in local surface water temperature partly control the

657   observed (semi-)diurnal variability in trace element concentrations in Red Sea tridacnids.

658   4.3.4 Seasonal variability and temperature relationships

659   On longer (seasonal) timescales, Sr/Ca in tridacnids has been suggested as a temperature proxy

660   similar to the well-known Sr/Ca-Sea Surface Temperature relationship in tropical corals (Lough,

661   2010; Yan et al., 2013). However, significantly lower Sr/Ca ratios in tridacnids compared to coral

662   aragonite (1.5 – 2.0 mmol/mol vs. 7.5 – 9.5 mmol/mol in corals; (Elliot et al., 2009); **Fig. 2**) suggest

663   that tridacnids exert a large degree of biological control on the Sr concentration in their shells,

664   either through the light-sensitive photosymbiosis-calcification relationship outlined above

665   (**section 4.3.2**) or otherwise through active Sr removal from the biomineralization site by Sr-

666   binding organic molecules (following the model proposed by (Gillikin et al., 2005)). Similarly,

667   Mg/Ca ratios in tridacnids were previously thought to primarily record water temperature (e.g.,

668   (Batenburg et al., 2011)) but our detailed investigation shows large differences in Mg

669   concentration within tridacnid shells and a strong anticorrelation of Mg with sulfur compounds

670   associated with the organic matrix in the shell (see **section 4.2.1**; (Dauphin et al., 2003)), has

671   been put forward as evidence for a strong control of calcification and microstructure on Mg

672   composition in tridacnid shells (Yoshimura et al., 2014). However, evidence from studies on

673   foraminifera calcification demonstrate that the sulfur in biocarbonates is not organically bound

674   and that the covariation with Mg might instead be caused by lattice distortion due to incorporation

675   of Mg favoring simultaneous S incorporation (van Dijk et al., 2017). If this is also the case in

676   tridacnids, the Mg/Ca-S/Ca covariance observed in previous studies might not preclude the use

677   of Mg/Ca as a temperature proxy. In that case, more detailed calibration studies (e.g. using

678   controlled growth experiments; (Warter et al., 2018)) are required to establish this proxy.

679   4.3.5 Ba/Ca and Mn/Ca in tridacnids

680   As in the pectinids, Ba/Ca ratios in tridacnids likely reflect changes in Ba concentration in the

681   environment, which can be caused by river input, upwelling of comparatively nutrient-rich waters

682   or blooms of Ba-rich phytoplankton (Vander Putten et al., 2000; Elliot et al., 2009). Given that Mn

683   is mostly associated with the mineral fraction of bivalve shells and seems to fractionate into the

684   shell close to equilibrium with seawater (Onuma et al., 1979; Soldati et al., 2016), Mn/Ca ratios in

685   tridacnids likely reflect the availability of dissolved Mn in the water column, as in other mollusk

686   taxa (e.g., (Barats et al., 2009); see **section 4.2**). This assumption is supported by the correlation

687   between Mn/Ca and Ba/Ca measured in this study (**Fig. 2**), suggesting that both records are

688   influenced on seasonal timescales by variability in nutrient availability and redox conditions (*sensu*

689   (Dehairs et al., 1989)). Part of this correlation between Mn/Ca and Ba/Ca is driven by synchronous

690   increases in both elements near the start and end of the profiles through tridacnid shells (**Fig. 2**).

691   These changes may reflect a decrease of control on shell composition during periods of stress,

692   or alternatively reflect periods of slower growth which cause more primitive microstructures

693   (characterized by higher concentrations of trace elements) to be formed (Warter et al., 2018).

694   4.2.6 Environmental changes in the Gulf of Aqaba

695   Given that the Gulf of Aqaba is oligotrophic, seasonally stratified, and lacks significant riverine

696   input (Nassar et al., 2014; Manasrah et al., 2019), the variability in nutrient concentrations and

697   redox conditions driving Mn/Ca and Ba/Ca variability in tridacnids are likely driven by convective

698   overturning. The tidal amplitude is much smaller than in the Bay of Brest (< 1 m; (Manasrah et al.,

699   2019)) and is unlikely to drive significant short-term fluctuations in sea water chemistry. This may

700   therefore explain the lack of tidal (12 h) periodicity in Ba/Ca and Mn/Ca in tridacnids (**Fig. 5-6**) .

701   Nevertheless, tidal rhythms have been observed in the behavior and growth of deep-sea bivalves

702   living far below the direct influence of tides on the environment, proving that such patterns can be

703   recorded by the animals through their circadian rhythm (Schöne and Giere, 2005; Nedoncelle et

704   al., 2013; Mat et al., 2020). In this case, the daily cycle seems to have been more important for

Ba/Ca in tridacnids, plausibly by driving diurnal changes in primary productivity in the Gulf of Aqaba. Alternatively, the daily periodicity found in tridacnid shell chemistry may in fact be a response to the lunar day (~24.8 h) cycle, which is imprinted in the shell's chemical composition through periodic exposure of the clams to extreme heat or air (subaerial exposure) in their shallow water environment during exceptionally low tides. The stress induced from this exposure could have affected calcification and incorporation of trace elements (see **section 4.3.5**).

Interestingly, Sr/Ca ratios in tridacnids do exhibit tidal periodicity (**Table 2**; **Fig. 3**), perhaps driven by a circadian rhythm in calcification linked to the tidal cycle, or by subtle changes in water temperature driven by tidal currents (Carlson et al., 2014). This 12 h periodic behavior is not observed in previous studies of Sr/Ca ratios in tridacnids (Sano et al., 2012; Warter et al., 2018). A recent valvometric study on tridacnids found a 12 h period in activity, which supports the hypothesis that a circadian rhythm paced to the tidal cycle could influence shell calcification (Killam and Clapham, 2018b). Significant daily fluctuations in solar radiation (up to 1500 W m^{-2}; (Manasrah et al., 2019)) likely exert control on the calcification of tridacnids in the Red Sea, explaining the strong diurnal periodicity in Sr/Ca and Ba/Ca records in this study (see **Fig. 6** and **Fig. 8**). As in the (non-symbiotic) pectinid data, it seems likely that the majority of Mn/Ca and Ba/Ca variability in tridacnids directly reflects changes in the chemistry of the sea water and its constituents (e.g., particulate organic matter) while Mg/Ca and Sr/Ca variations are driven by changes in calcification and microstructure. The latter may be indirectly influenced by light intensity through photosynthesis by the symbionts, or by circadian rhythms paces to the diurnal or tidal cycle.

4.4 Role of photosymbiosis on high-frequency chemical variability

4.4.1 Effect of symbiosis on shell formation

729   While the amplitude of diurnal variability in trace element concentrations does not vary much

730   between the symbiotic tridacnids and the non-symbiotic pectinids (**Fig. 6**), the amount of variance

731   in the trace element records explained by daily cyclicity is up to twice as high in tridacnids (**Fig.**

732   **7**; **Table 3**). This suggests that the 24 h cycle has a much larger relative influence on trace

733   element composition (especially Sr/Ca and Ba/Ca) in tridacnids than in pectinids. This seems to

734   point towards a role of the photosymbionts in calcification by tridacnids, such as through symbiont-

735   mediated diurnal variation in the pH of the extrapallial fluid (Ip et al., 2006), as well as active

736   transport of HCO_3^- for calcification (Chew et al., 2019) and as a C supply to the symbionts from

737   the host (Boo et al., 2021). Given the differences in elemental ratios between these two groups

738   of bivalves, comparing variance yields a more robust assessment of the relative importance of

739   tidal or diurnal variability on shell composition than looking at the absolute size (amplitude) of the

740   chemical cycle. While the difference in variance is clear, the importance of diurnal cyclicity on the

741   photosymbiotic tridacnids is not as big as one might expect. Rarely more than 10 % of the variance

742   is explained by day-night variability (**Table 3**). This seems to contradict the large daily Sr/Ca

743   amplitudes found in (Warter et al., 2018) and the trace element fluctuations found in (de Winter

744   et al., 2020), which rival the seasonal cycle in these trace element ratios in terms of amplitude.

745   However, the percentages in **Table 3** relate to the amount of variation in the complete records

746   through these individuals and therefore also contain areas of the shell where daily cyclicity is less

747   pronounced, while values in previous studies often reflect maximum amplitudes recorded in parts

748   of the shell with exceptionally clear daily increments.

749   4.4.2 Effect of differences in the environment

750   It seems plausible that part of the difference in diurnal variability between pectinids and tridacnids

751   is explained by a difference in the environment between the Gulf of Aqaba and the Bay of Brest,

752   rather than the presence of photosymbionts. The diurnal insolation cycle in the Gulf of Aqaba is

753   larger than in the Bay of Brest (1500 vs 546 $W*m^{-2}$ maximum summer irradiance; (Roberts et al.,

754 2018; Manasrah et al., 2019)). If calcification in pectinids would be equally sensitive to sunlight,

755 this difference may explain much of the difference between the species. In this scenario, part of

756 the strong tidal component in the pectinid trace element data may be explained by the influence

757 of differences in water depth on the penetration of sunlight through the murky waters of the Bay

758 of Brest (Roberts et al., 2018). In fact, tidal movement can cause strong non-linear amplification

759 or reduction of the solar irradiance at the sea floor of the Bay of Brest by factors exceeding 10,

760 especially outside the summer months, which in turn has a significant effect on primary

761 productivity in the water column (Roberts et al., 2018). This tidal effect is likely to be much weaker

762 in the Gulf of Aqaba, given its comparatively low tidal amplitude, clear oligotrophic waters, and

763 much stronger and less seasonal day-night cycle (Manasrah et al., 2019). Indeed, even in non-

764 photosymbiotic bivalves, light and food availability are demonstrated to be major drivers of the

765 animal's behavior (e.g., (Ballesta-Artero et al., 2017)). The combination of the daily and tidal

766 cycles on solar irradiance at depth and photosynthesis in the Bay of Brest may therefore pose an

767 alternative pathway for strong tidal cyclicity in the trace element composition of pectinids in this

768 study and account for part of the twofold increase in daily variability in tridacnids compared to the

769 pectinids (**Fig. 7-8**; **Table 3**).

770 4.4.3 Effect of direct insolation

771 Specimen **TSM1** poses an interesting case study for investigating the link between sunlight and

772 calcification in tridacnids, since it grew under a sunshade and therefore experienced a dampened

773 diurnal variability in insolation compared to other giant clams in the area. The fact that this

774 specimen exhibits similar or even higher diurnal variability in shell chemistry (**Fig. 7**) argues

775 against a direct influence of the rate of photosynthesis itself on calcification. Instead, it seems that

776 daily chemical variability is mostly an expression of circadian rhythm in tridacnids, which is

777 strongly (evolutionarily) coupled to the day-night cycle to optimize the symbiosis with primary

778 producers in its mantle, possibly through respiration rhythms carried out by the ctenidium (see

779 **section 4.3**; (Ip and Chew, 2021)). Symbionts have been shown to directly aid in calcification

780 through proton pumping (Armstrong et al., 2018), influencing internal acid-base chemistry (Ip et

781 al., 2006), and valvometric studies show the clams bask in sunlight in daylight hours and close

782 partially at night when symbiosis is likely reduced (Schwartzmann et al., 2011). This conclusion

783 is further supported by the lack of a clear difference in diurnal cyclicity between trace element

784 records in *T. maxima*, *T. squamosa* and *T. squamosina* (**Fig. 7**; **Table 3**), even though the degree

785 of reliance on photosymbiosis is demonstrated to be highly variable between these species

786 (Killam et al., 2020). Therefore, it seems unlikely that sub-daily resolved trace element records in

787 tridacnids can be used as quantitative recorders of paleo-insolation, as was originally suggested

788 by (Sano et al., 2012). While the degree of symbiotic activity may not be clearly recorded in the

789 daily amplitude of trace element oscillations, the consistency of daily periodic signal in the studied

790 giant clams could relate to the direct biological control exerted by the symbionts on the hosts'

791 rhythms of calcification. Light exposure in giant clams promotes expression of genes coding for

792 proteins involved in Ca^{2+}, H^+ and HCO_3^- transport in the mantles of giant clams (Ip et al., 2017;

793 Chew et al., 2019), with the expression proposed to be at least partially mediated by photosensing

794 on the part of the symbionts themselves (Ip et al., 2017). Differences between the daily

795 consistency (spectral power) of photosymbiotic and non-photosymbiotic trace element profiles

796 might still allow paleontologists to use the presence of strong daily periodicity as a proxy for

797 photosymbiosis in the fossil record (as suggested by (de Winter et al., 2020)). However, the small

798 differences found between pectinids and tridacnids in this study and the comparatively large

799 influence of environmental variability show that such records should be interpreted with caution.

800 Future studies could measure photosynthetic activity of the symbionts in tridacnids and attempt

801 to relate this to the trace element composition of the shell in an attempt to isolate the direct effect

802 of photosymbiosis on shell composition.

803

804   4.5 Aperiodic drivers of shell chemistry

805   4.5.1 Circadian and behavioral changes

806   Even after controlling for instrumental noise, most (~ 90 %) of the variance observed in our trace

807   element records is not directly related to the diurnal or tidal cycle. This suggests that aperiodic

808   events at the scale of hours to days play an important role in the calcification of pectinids and

809   tridacnids. Given the large difference in ecological niche (e.g., photosymbiotic versus non-

810   symbiotic) between these taxa, and the difference between the environment in which they grew,

811   this observation suggests that calcification of bivalves at the (sub-)daily scale is generally

812   dominated by aperiodic variability in calcification or in the environment. Part of this unaccounted

813   variability may be caused by variability in the animal's behavior, as documented by observations

814   of siphon and valve gape activity in cultured or monitored specimens of a variety of bivalve taxa

815   (Rodland et al., 2006; Ballesta-Artero et al., 2017). While these experiments revealed quasi-

816   periodic (3-7 minute and 60–90 minute periods) behavior unassociated with the tidal or daily cycle,

817   records of activity of the bivalves also reveal less regular patterns on the scale of 2–24 h which

818   may contribute to the aperiodic variance in trace element records (Rodland et al., 2006). Another

819   example of aperiodic behavior potentially influencing shell chemistry is rapid valve adduction or

820   "coughing" observed in both pectinids and tridacnids, which serves as a mechanism for expelling

821   respiratory CO_2 and faeces from the pallial cavity or to evade predation attempts (Robson et al.,

822   2012; Soo and Todd, 2014). This behavior could resuspend sediment and produce pulses of Mn

823   and Ba at the sediment-water interface which are recorded as short-term, aperiodic variability in

824   these elements in the shell. The temporal sampling resolution (several hours) of our trace element

825   records after smoothing out measurement noise does not allow us to resolve the types of periodic

826   variability at the sub-hourly scale cited in these previous studies, meaning that aperiodic variability

827   in behavior and aliasing of these ultradian patterns likely contribute to the aperiodic variability in

828   our trace element records. On longer (sub-)seasonal timescales, activity in bivalves is shown to

829   be highly dependent on food and light availability (Ballesta-Artero et al., 2017), suggesting that

830   aperiodic, short-term changes in these environmental factors could be a main driver of shell

831   growth and composition and explain a large part of the variance in the trace element records

832   which is not explained by ultradian changes in the animal's behavior.

833   4.5.2 Short-term environmental changes and paleoweather

834   Outside of regular fluctuations caused by tidal, daily, and seasonal cycles, changes in light and

835   food availability at the hourly to daily scale are probably linked to circulation and weather

836   phenomena. Previous studies show that enhanced vertical mixing during weather events such as

837   storms, algal bloom events after wind-driven upwelling and pseudoperiodic dust deposition can

838   temporarily increase the concentration of dissolved metals in surface waters, resuspend organic

839   matter and temporarily increase primary productivity (Lin et al., 2003; Al-Najjar et al., 2007; Iluz

840   et al., 2009; Al-Taani et al., 2015; Komagoe et al., 2018). This will in turn lead to a shallowing of

841   the redoxcline through increased organic matter load at the sediment-water interface, which can

842   be recorded in the composition of giant clam shells (Yan et al., 2020). Interestingly, data in (Yan

843   et al., 2020) suggest that recording an extreme weather event in *Tridacna* requires wind speeds

844   exceeding 20 km/h, a threshold which is almost never reached in the comparatively quiet Gulf of

845   Aqaba (Manasrah et al., 2019), while such events are common in the stormier Bay of Brest (Hily

846   et al., 1992; Chauvaud et al., 2005). This difference is also reflected in the periodicity of shell

847   composition, with the tridacnids having overall higher percentages of their variance explained by

848   daily and tidal variability than pectinids (**Fig. 3 and 7**), showing that aperiodic (potentially weather-

849   controlled) variability in shell composition has a stronger influence on the pectinids which grew in

850   the stormier Bay of Brest. A plausible scenario therefore emerges in which aperiodic weather

851   events cause short-term variability in both the chemistry and physical properties of the water

852   column. These changes are subsequently recorded in bivalve shells, either directly because the

853   weather events resuspend, remobilize or deliver trace elements like Mn and Ba (e.g., (Dehairs et

854   al., 1989; Gillikin et al., 2008; Mahé et al., 2010)), or indirectly because environmental stress

855   associated with the event affects behavior and shell calcification, resulting in a change in the

856   incorporation of alkali-group cations (e.g., Mg and Sr) into the shell biomineral ((Carré et al., 2006;

857   Takesue et al., 2008); **Fig. 8**). Our results therefore highlight the potential of high-resolution trace

858   element records in bivalve shells to record short-term circulation changes and weather events,

859   while prescribing caution in interpreting such records until the effect of true environmental

860   changes on the sub-daily scale can be separated from aperiodic ultradian or behavioral patterns.

861

5. Conclusions

Our high-resolution trace element records reveal that short-term variability on the tidal or daily scale is recorded in the Mg, Sr, Mn, and Ba composition of shells of fast-growing mollusk species. The application of spectral analysis and variance decomposition on these trace element records is a useful tool to assess the influence of periodicity in the shallow marine environment on calcification in mollusk shells. Our statistical analysis reveals that tidal and daily variability on average account for less than 10 % of trace element variance in pectinids and tridacnids. In photosymbiotic giant clam shells, the amount of variance in Sr and Ba paced to the daily cycle is two times higher than in the non-photosymbiotic pectinids, suggesting that photosymbiosis in giant clams exerts some control on trace element composition in their shells. However, since only ~10 % of the trace element variability in tridacnids is explained by diurnal variability, the recognition of photosymbiosis in the fossil record from diurnal variability in fossil shell composition will be complicated. In addition, differences between the mid-latitude environment of the pectinids and the tropical environment of the tridacnids likely account for part of the difference in trace element composition between the taxa.

We propose that Ba and Mn composition in pectinids and tridacnids reflect short-term variability in primary productivity and sea water chemistry which control the mobility of these elements. Concentrations of Mg and Sr are likely controlled by short-term changes in growth and metabolic rate of the mollusks, which may be indirectly controlled by changes in their environment through circadian rhythms or behavior, explaining the pacing of trace element composition to the tidal and diurnal cycle. Most of the variance in trace element records in both taxa are not related to periodic behavior at the 12 h or 24 h scale, likely recording aperiodic events in the environment related to weather-scale phenomena or circadian patterns. We thus conclude that mollusk shell carbonate is a promising archive for recording weather-scale variability in shallow marine environments

886   across latitudes, potentially recording weather-scale phenomena in deep time, as long as these

887   environmental effects can be separated by the influence of the behavior of the animal.

888

889   **Code availability**

890   Scripts used for data processing and to create figures in this manuscript were uploaded to an

891   open-access repository on GitHub (https://github.com/nielsjdewinter/TE_circadian) and linked

892   through Zenodo (https://zenodo.org/record/6603175).

893

894   **Data availability**

895   Supplementary data and figures referenced in this contribution were uploaded to the online open-

896   access repository Zenodo (https://doi.org/10.5281/zenodo.6602894).

897

898   **Author contribution**

899   NJW designed the experiment after discussion with BRS, DK and LF. LF, DK, BRS and JT

900   collected the samples. LF, DK and NJW together prepared samples for analyses and constructed

901   shell chronologies using growth line counting. WB, LN, GJR and NJW carried out the LA-ICP-MS

902   analyses and data processing. NJW designed and carried out the statistical analyses and wrote

903   the R scripts guided by feedback from LN, BK, LN, WB and GJR. NJW wrote the first draft of the

904   manuscript. All authors contributed to the writing process towards the final version of the

905   manuscript.

906

907   **Competing interests**

908   The authors declare that they have no conflict of interest.

909   **Acknowledgements**

910   The authors would like to thank Leonard Bik for his help with sample preparation and Maarten

911   Zeilmans for his help with high-resolution imaging of the samples at Utrecht University. This study

912   is part of the UNBIAS project, jointly funded by a Flemish Research Foundation (FWO;

913   12ZB220N) post-doctoral fellowship (NJW) and a MSCA Individual Fellowship (H2020-MSCA-IF-

914   2018; 843011 – UNBIAS; awarded to NJW). GJR and LKD acknowledge funding from the

915   Netherlands Earth System Science Center (NESSC; grant no. 024.002.001) from the Dutch

916   Ministry for Education, Culture and Science (gravitation grant no. NWO 024.002.001). BRS

917   acknowledges funding from the Deutsche Forschungsgemeinschaft (DFG; SCHO 793/21

918   [HIPPO]+ SCHO 793/23). JT acknowledges funding from the French National Research Agency

919   (ANR; ANR-18-CE92-0036-01) awarded within the framework of the French-German

920   collaborative project HIPPO (HIgh-resolution Primary Production multiprOxy archives).

921

922   **References**

923   Agbaje, O. B. A., Wirth, R., Morales, L. F. G., Shirai, K., Kosnik, M., Watanabe, T., and Jacob, D. E.:
924   Architecture of crossed-lamellar bivalve shells: the southern giant clam (Tridacna derasa, Röding, 1798),
925   R. Soc. Open Sci., 4, 170622, https://doi.org/10.1098/rsos.170622, 2017.

926   Al-Aasm, I. S. and Veizer, J.: Diagenetic stabilization of aragonite and low-Mg calcite, I. Trace elements in
927   rudists, J. Sediment. Res., 56, 138–152, 1986a.

928   Al-Aasm, I. S. and Veizer, J.: Diagenetic stabilization of aragonite and low-Mg calcite, II. Stable isotopes in
929   rudists, J. Sediment. Res., 56, 1986b.

930   Al-Najjar, T., Badran, M. I., Richter, C., Meyerhoefer, M., and Sommer, U.: Seasonal dynamics of
931   phytoplankton in the Gulf of Aqaba, Red Sea, Hydrobiologia, 579, 69–83,
932   https://doi.org/10.1007/s10750-006-0365-z, 2007.

933   Al-Taani, A. A., Rashdan, M., and Khashashneh, S.: Atmospheric dry deposition of mineral dust to the
934   Gulf of Aqaba, Red Sea: Rate and trace elements, Mar. Pollut. Bull., 92, 252–258,
935   https://doi.org/10.1016/j.marpolbul.2014.11.047, 2015.

Anand, P. and Elderfield, H.: Variability of Mg/Ca and Sr/Ca between and within the planktonic foraminifers Globigerina bulloides and Globorotalia truncatulinoides, Geochem. Geophys. Geosystems, 6, https://doi.org/10.1029/2004GC000811, 2005.

Armstrong, E. J., Roa, J. N., Stillman, J. H., and Tresguerres, M.: Symbiont photosynthesis in giant clams is promoted by V-type H+-ATPase from host cells, J. Exp. Biol., 221, jeb177220, https://doi.org/10.1242/jeb.177220, 2018.

Ballesta-Artero, I., Witbaard, R., Carroll, M. L., and van der Meer, J.: Environmental factors regulating gaping activity of the bivalve Arctica islandica in Northern Norway, Mar. Biol., 164, 116, 2017.

Barats, A., Amouroux, D., Pécheyran, C., Chauvaud, L., and Donard, O. F. X.: High-Frequency Archives of Manganese Inputs To Coastal Waters (Bay of Seine, France) Resolved by the LA–ICP–MS Analysis of Calcitic Growth Layers along Scallop Shells (Pecten maximus), Environ. Sci. Technol., 42, 86–92, https://doi.org/10.1021/es0701210, 2008.

Barats, A., Amouroux, D., Chauvaud, L., Pécheyran, C., Lorrain, A., Thébault, J., Church, T. M., and Donard, O. F. X.: High frequency Barium profiles in shells of the Great Scallop *Pecten maximus*: a methodical long-term and multi-site survey in Western Europe, Biogeosciences, 6, 157–170, https://doi.org/10.5194/bg-6-157-2009, 2009.

Batenburg, S. J., Reichart, G.-J., Jilbert, T., Janse, M., Wesselingh, F. P., and Renema, W.: Interannual climate variability in the Miocene: High resolution trace element and stable isotope ratios in giant clams, Palaeogeogr. Palaeoclimatol. Palaeoecol., 306, 75–81, 2011.

Black, B. A.: Climate-driven synchrony across tree, bivalve, and rockfish growth-increment chronologies of the northeast Pacific, Mar. Ecol. Prog. Ser., 378, 37–46, 2009.

Boo, M. V., Chew, S. F., and Ip, Y. K.: The colorful mantle of the giant clam Tridacna squamosa expresses a homolog of electrogenic sodium: Bicarbonate cotransporter 2 that mediates the supply of inorganic carbon to photosynthesizing symbionts, PloS One, 16, e0258519, https://doi.org/10.1371/journal.pone.0258519, 2021.

Bougeois, L., De Rafélis, M., Reichart, G.-J., De Nooijer, L. J., Nicollin, F., and Dupont-Nivet, G.: A high resolution study of trace elements and stable isotopes in oyster shells to estimate Central Asian Middle Eocene seasonality, Chem. Geol., 363, 200–212, 2014.

Carlson, D. F., Fredj, E., and Gildor, H.: The annual cycle of vertical mixing and restratification in the Northern Gulf of Eilat/Aqaba (Red Sea) based on high temporal and vertical resolution observations, Deep Sea Res. Part Oceanogr. Res. Pap., 84, 1–17, https://doi.org/10.1016/j.dsr.2013.10.004, 2014.

Carré, M., Bentaleb, I., Bruguier, O., Ordinola, E., Barrett, N. T., and Fontugne, M.: Calcification rate influence on trace element concentrations in aragonitic bivalve shells: Evidences and mechanisms, Geochim. Cosmochim. Acta, 70, 4906–4920, https://doi.org/10.1016/j.gca.2006.07.019, 2006.

Chauvaud, L., Lorrain, A., Dunbar, R. B., Paulet, Y.-M., Thouzeau, G., Jean, F., Guarini, J.-M., and Mucciarone, D.: Shell of the Great Scallop Pecten maximus as a high-frequency archive of paleoenvironmental changes, Geochem. Geophys. Geosystems, 6, 2005.

973 Checa, A. G., Esteban-Delgado, F. J., and Rodríguez-Navarro, A. B.: Crystallographic structure of the
974 foliated calcite of bivalves, J. Struct. Biol., 157, 393–402, 2007.

975 Chew, S. F., Koh, C. Z., Hiong, K. C., Choo, C. Y., Wong, W. P., Neo, M. L., and Ip, Y. K.: Light-enhanced
976 expression of Carbonic Anhydrase 4-like supports shell formation in the fluted giant clam Tridacna
977 squamosa, Gene, 683, 101–112, 2019.

978 Cochran, J. K., Kallenberg, K., Landman, N. H., Harries, P. J., Weinreb, D., Turekian, K. K., Beck, A. J., and
979 Cobban, W. A.: Effect of diagenesis on the Sr, O, and C isotope composition of late Cretaceous mollusks
980 from the Western Interior Seaway of North America, Am. J. Sci., 310, 69–88,
981 https://doi.org/10.2475/02.2010.01, 2010.

982 Cohen, A. L., Owens, K. E., Layne, G. D., and Shimizu, N.: The Effect of Algal Symbionts on the Accuracy of
983 Sr/Ca Paleotemperatures from Coral, Science, 296, 331–333, https://doi.org/10.1126/science.1069330,
984 2002.

985 Coimbra, J., Machado, J., Fernandes, P. L., Ferreira, H. G., and Ferreira, K. G.: Electrophysiology of the
986 Mantle of Anodonta Cygnea, J. Exp. Biol., 140, 65–88, https://doi.org/10.1242/jeb.140.1.65, 1988.

987 Coimbra, R., Huck, S., de Winter, N. J., Heimhofer, U., and Claeys, P.: Improving the detection of shell
988 alteration: Implications for sclerochronology, Palaeogeogr. Palaeoclimatol. Palaeoecol., 559, 109968,
989 https://doi.org/10.1016/j.palaeo.2020.109968, 2020.

990 Comboul, M., Emile-Geay, J., Evans, M. N., Mirnateghi, N., Cobb, K. M., and Thompson, D. M.: A
991 probabilistic model of chronological errors in layer-counted climate proxies: applications to annually
992 banded coral archives, Clim. Past, 10, 825–841, 2014.

993 Crippa, G., Griesshaber, E., Checa, A. G., Harper, E. M., Roda, M. S., and Schmahl, W. W.: Orientation
994 patterns of aragonitic crossed-lamellar, fibrous prismatic and myostracal microstructures of modern
995 Glycymeris shells, J. Struct. Biol., 212, 107653, 2020.

996 Dauphin, Y., Cuif, J., Doucet, J., Salomé, M., Susini, J., and Williams, C.: In situ mapping of growth lines in
997 the calcitic prismatic layers of mollusc shells using X-ray absorption near-edge structure (XANES)
998 spectroscopy at the sulphur K-edge, Mar. Biol., 142, 299–304, 2003.

999 Day, C. C. and Henderson, G. M.: Controls on trace-element partitioning in cave-analogue calcite,
1000 Geochim. Cosmochim. Acta, 120, 612–627, https://doi.org/10.1016/j.gca.2013.05.044, 2013.

1001 DeCarlo, T. M. and Cohen, A. L.: Dissepiments, density bands and signatures of thermal stress in Porites
1002 skeletons, Coral Reefs, 36, 749–761, https://doi.org/10.1007/s00338-017-1566-9, 2017.

1003 Dehairs, F., Baeyens, W., and Van Gansbeke, D.: Tight coupling between enrichment of iron and
1004 manganese in North Sea suspended matter and sedimentary redox processes: Evidence for seasonal
1005 variability, Estuar. Coast. Shelf Sci., 29, 457–471, https://doi.org/10.1016/0272-7714(89)90080-2, 1989.

1006 van Dijk, I., de Nooijer, L. J., Boer, W., and Reichart, G.-J.: Sulfur in foraminiferal calcite as a potential
1007 proxy for seawater carbonate ion concentration, Earth Planet. Sci. Lett., 470, 64–72, 2017.

Dunbar, R. B. and Wellington, G. M.: Stable isotopes in a branching coral monitor seasonal temperature variation, Nature, 293, 453–455, 1981.

Eggins, S., De Deckker, P., and Marshall, J.: Mg/Ca variation in planktonic foraminifera tests: implications for reconstructing palaeo-seawater temperature and habitat migration, Earth Planet. Sci. Lett., 212, 291–306, https://doi.org/10.1016/S0012-821X(03)00283-8, 2003.

Elliot, M., Welsh, K., Chilcott, C., McCulloch, M., Chappell, J., and Ayling, B.: Profiles of trace elements and stable isotopes derived from giant long-lived Tridacna gigas bivalves: potential applications in paleoclimate studies, Palaeogeogr. Palaeoclimatol. Palaeoecol., 280, 132–142, 2009.

Freitas, P. S., Clarke, L. J., Kennedy, H., Richardson, C. A., and others: Ion microprobe assessment of the heterogeneity of Mg/Ca, Sr/Ca and Mn/Ca ratios in Pecten maximus and Mytilus edulis (bivalvia) shell calcite precipitated at constant temperature, Biogeosciences Discuss., 6, 1267, 2009.

Fröhlich, L., Siebert, V., Walliser, E. O., Thébault, J., Jochum, K. P., Chauvaud, L., and Schöne, B. R.: Ba/Ca profiles in shells of Pecten maximus – A proxy for specific primary producers rather than bulk phytoplankton, Chem. Geol., 120743, https://doi.org/10.1016/j.chemgeo.2022.120743, 2022.

Gannon, M. E., Pérez-Huerta, A., Aharon, P., and Street, S. C.: A biomineralization study of the Indo-Pacific giant clam Tridacna gigas, Coral Reefs, 36, 503–517, https://doi.org/10.1007/s00338-016-1538-5, 2017.

García-March, J. R., Sanchís Solsona, M. Á., and García-Carrascosa, A. M.: Shell gaping behaviour of Pinna nobilis L., 1758: circadian and circalunar rhythms revealed by in situ monitoring, Mar. Biol., 153, 689–698, https://doi.org/10.1007/s00227-007-0842-6, 2008.

Gilbert, P. U., Bergmann, K. D., Myers, C. E., Marcus, M. A., DeVol, R. T., Sun, C.-Y., Blonsky, A. Z., Tamre, E., Zhao, J., and Karan, E. A.: Nacre tablet thickness records formation temperature in modern and fossil shells, Earth Planet. Sci. Lett., 460, 281–292, 2017.

Gillikin, D. P., Lorrain, A., Navez, J., Taylor, J. W., André, L., Keppens, E., Baeyens, W., and Dehairs, F.: Strong biological controls on Sr/Ca ratios in aragonitic marine bivalve shells, Geochem. Geophys. Geosystems, 6, https://doi.org/10.1029/2004GC000874, 2005.

Gillikin, D. P., Lorrain, A., Paulet, Y.-M., André, L., and Dehairs, F.: Synchronous barium peaks in high-resolution profiles of calcite and aragonite marine bivalve shells, Geo-Mar. Lett., 28, 351–358, 2008.

Goodwin, D. H., Paul, P., and Wissink, C. L.: MoGroFunGen: A numerical model for reconstructing intra-annual growth rates of bivalve molluscs, Palaeogeogr. Palaeoclimatol. Palaeoecol., 276, 47–55, https://doi.org/10.1016/j.palaeo.2009.02.026, 2009.

Guillaume Olivier, M., Leroux, E., Rabineau, M., Le Hir, P., Granjeon, D., Chataigner, T., Beudin, A., and Muller, H.: Numerical modelling of a Macrotidal Bay over the last 9,000 years: An interdisciplinary methodology to understand the influence of sea-level variations on tidal currents in the Bay of Brest, Cont. Shelf Res., 231, 104595, https://doi.org/10.1016/j.csr.2021.104595, 2021.

1043 Guillong, M., Meier, D. L., Allan, M. M., Heinrich, C. A., and Yardley, B. W. D.: SILLS: A Matlab-based
1044 program for the reduction of laser ablation ICP–MS data of homogenous materials and inclusions,
1045 Mineral. Assoc. Can. Short Course, 40, 328–333, 2008.

1046 Hagiwara, S. and Byerly, L.: Calcium channel, Annu. Rev. Neurosci., 4, 69–125, 1981.

1047 Hallmann, N., Schöne, B. R., Strom, A., and Fiebig, J.: An intractable climate archive—Sclerochronological
1048 and shell oxygen isotope analyses of the Pacific geoduck, Panopea abrupta (bivalve mollusk) from
1049 Protection Island (Washington State, USA), Palaeogeogr. Palaeoclimatol. Palaeoecol., 269, 115–126,
1050 2008.

1051 Hily, C., Potin, P., and Floc'h, J.-Y.: Structure of subtidal algal assemblages on soft-bottom sediments:
1052 fauna/flora interactions and role of disburbances in the Bay of Brest, France, Mar. Ecol. Prog. Ser., 85,
1053 115–130, 1992.

1054 Höche, N., Peharda, M., Walliser, E. O., and Schöne, B. R.: Morphological variations of crossed-lamellar
1055 ultrastructures of Glycymeris bimaculata (Bivalvia) serve as a marine temperature proxy, Estuar. Coast.
1056 Shelf Sci., 237, 106658, https://doi.org/10.1016/j.ecss.2020.106658, 2020.

1057 Höche, N., Walliser, E. O., de Winter, N. J., Witbaard, R., and Schöne, B. R.: Temperature-induced
1058 microstructural changes in shells of laboratory-grown Arctica islandica (Bivalvia), PloS One, 16,
1059 e0247968, 2021.

1060 Huyghe, D., de Rafelis, M., Ropert, M., Mouchi, V., Emmanuel, L., Renard, M., and Lartaud, F.: New
1061 insights into oyster high-resolution hinge growth patterns, Mar. Biol., 166, 48, 2019.

1062 Huyghe, D., Daëron, M., de Rafelis, M., Blamart, D., Sébilo, M., Paulet, Y.-M., and Lartaud, F.: Clumped
1063 isotopes in modern marine bivalves, Geochim. Cosmochim. Acta, 316, 41–58,
1064 https://doi.org/10.1016/j.gca.2021.09.019, 2021.

1065 Iluz, D., Dishon, G., Capuzzo, E., Meeder, E., Astoreca, R., Montecino, V., Znachor, P., Ediger, D., and
1066 Marra, J.: Short-term variability in primary productivity during a wind-driven diatom bloom in the Gulf of
1067 Eilat (Aqaba), Aquat. Microb. Ecol., 56, 205–215, https://doi.org/10.3354/ame01321, 2009.

1068 Inoue, M., Nakamura, T., Tanaka, Y., Suzuki, A., Yokoyama, Y., Kawahata, H., Sakai, K., and Gussone, N.: A
1069 simple role of coral-algal symbiosis in coral calcification based on multiple geochemical tracers,
1070 Geochim. Cosmochim. Acta, 235, 76–88, https://doi.org/10.1016/j.gca.2018.05.016, 2018.

1071 Ip, Y. K. and Chew, S. F.: Light-Dependent Phenomena and Related Molecular Mechanisms in Giant
1072 Clam-Dinoflagellate Associations: A Review, Front. Mar. Sci., 8, 2021.

1073 Ip, Y. K., Loong, A. M., Hiong, K. C., Wong, W. P., Chew, S. F., Reddy, K., Sivaloganathan, B., and
1074 Ballantyne, J. S.: Light induces an increase in the pH of and a decrease in the ammonia concentration in
1075 the extrapallial fluid of the giant clam Tridacna squamosa, Physiol. Biochem. Zool., 79, 656–664, 2006.

1076 Ip, Y. K., Koh, C. Z., Hiong, K. C., Choo, C. Y., Boo, M. V., Wong, W. P., Neo, M. L., and Chew, S. F.:
1077 Carbonic anhydrase 2-like in the giant clam, Tridacna squamosa: characterization, localization, response
1078 to light, and possible role in the transport of inorganic carbon from the host to its symbionts, Physiol.
1079 Rep., 5, e13494, 2017.

1080   Ivany, L. C.: Reconstructing paleoseasonality from accretionary skeletal carbonates—challenges and
1081   opportunities, Paleontol. Soc. Pap., 18, 133–166, 2012.

1082   Ivany, L. C. and Judd, E. J.: Deciphering Temperature Seasonality in Earth's Ancient Oceans, Annu. Rev.
1083   Earth Planet. Sci., 50, 123–152, https://doi.org/10.1146/annurev-earth-032320-095156, 2022.

1084   Jablonski, D., Roy, K., Valentine, J. W., Price, R. M., and Anderson, P. S.: The Impact of the Pull of the
1085   Recent on the History of Marine Diversity, Science, 300, 1133–1135,
1086   https://doi.org/10.1126/science.1083246, 2003.

1087   Jablonski, D., Huang, S., Roy, K., and Valentine, J. W.: Shaping the latitudinal diversity gradient: new
1088   perspectives from a synthesis of paleobiology and biogeography, Am. Nat., 189, 1–12, 2017.

1089   Jochum, K. P., Willbold, M., Raczek, I., Stoll, B., and Herwig, K.: Chemical Characterisation of the USGS
1090   Reference Glasses GSA-1G, GSC-1G, GSD-1G, GSE-1G, BCR-2G, BHVO-2G and BIR-1G Using EPMA, ID-
1091   TIMS, ID-ICP-MS and LA-ICP-MS, Geostand. Geoanalytical Res., 29, 285–302,
1092   https://doi.org/10.1111/j.1751-908X.2005.tb00901.x, 2005.

1093   Jochum, K. P., Weis, U., Stoll, B., Kuzmin, D., Yang, Q., Raczek, I., Jacob, D. E., Stracke, A., Birbaum, K.,
1094   and Frick, D. A.: Determination of reference values for NIST SRM 610–617 glasses following ISO
1095   guidelines, Geostand. Geoanalytical Res., 35, 397–429, 2011.

1096   Jones, D. S.: Sclerochronology: reading the record of the molluscan shell: annual growth increments in
1097   the shells of bivalve molluscs record marine climatic changes and reveal surprising longevity, Am. Sci.,
1098   71, 384–391, 1983.

1099   Jones, D. S. and Quitmyer, I. R.: Marking Time with Bivalve Shells: Oxygen Isotopes and Season of Annual
1100   Increment Formation, PALAIOS, 11, 340–346, https://doi.org/10.2307/3515244, 1996.

1101   Judd, E. J., Wilkinson, B. H., and Ivany, L. C.: The life and time of clams: Derivation of intra-annual growth
1102   rates from high-resolution oxygen isotope profiles, Palaeogeogr. Palaeoclimatol. Palaeoecol., 490, 70–
1103   83, 2018.

1104   Killam, D., Thomas, R., Al-Najjar, T., and Clapham, M.: Interspecific and Intrashell Stable Isotope
1105   Variation Among the Red Sea Giant Clams, Geochem. Geophys. Geosystems, 21, e2019GC008669,
1106   https://doi.org/10.1029/2019GC008669, 2020.

1107   Killam, D., Al-Najjar, T., and Clapham, M.: Giant clam growth in the Gulf of Aqaba is accelerated
1108   compared to fossil populations, Proc. R. Soc. B Biol. Sci., 288, 20210991,
1109   https://doi.org/10.1098/rspb.2021.0991, 2021.

1110   Killam, D. E. and Clapham, M. E.: Identifying the ticks of bivalve shell clocks: Seasonal growth in relation
1111   to temperature and food supply, PALAIOS, 33, 228–236, https://doi.org/10.2110/palo.2017.072, 2018a.

1112   Killam, D. E. and Clapham, M. E.: IDENTIFYING THE TICKS OF BIVALVE SHELL CLOCKS: SEASONAL
1113   GROWTH IN RELATION TO TEMPERATURE AND FOOD SUPPLY, PALAIOS, 33, 228–236,
1114   https://doi.org/10.2110/palo.2017.072, 2018b.

1115   Klein, R. T., Lohmann, K. C., and Thayer, C. W.: Bivalve skeletons record sea-surface temperature and
1116   δ18O via Mg/Ca and 18O/16O ratios, Geology, 24, 415–418, 1996.

1117   Komagoe, T., Watanabe, T., Shirai, K., Yamazaki, A., and Uematu, M.: Geochemical and Microstructural
1118   Signals in Giant Clam Tridacna maxima Recorded Typhoon Events at Okinotori Island, Japan, J. Geophys.
1119   Res. Biogeosciences, 123, 1460–1474, https://doi.org/10.1029/2017JG004082, 2018.

1120   Kontoyannis, C. G. and Vagenas, N. V.: Calcium carbonate phase analysis using XRD and FT-Raman
1121   spectroscopy, Analyst, 125, 251–255, https://doi.org/10.1039/A908609I, 2000.

1122   Ku, H. H.: Notes on the use of propagation of error formulas, J. Res. Natl. Bur. Stand., 70, 263–273, 1966.

1123   Lazareth, C. E., Vander Putten, E., André, L., and Dehairs, F.: High-resolution trace element profiles in
1124   shells of the mangrove bivalve Isognomon ephippium: a record of environmental spatio-temporal
1125   variations?, Estuar. Coast. Shelf Sci., 57, 1103–1114, 2003.

1126   Lazareth, C. E., Guzman, N., Poitrasson, F., Candaudap, F., and Ortlieb, L.: Nyctemeral variations of
1127   magnesium intake in the calcitic layer of a Chilean mollusk shell (Concholepas concholepas,
1128   Gastropoda), Geochim. Cosmochim. Acta, 71, 5369–5383, 2007.

1129   Lazier, A. V., SMITH, J. E., RISK, M. J., and SCHWARCZ, H. P.: The skeletal structure of Desmophyllum
1130   cristagalli: the use of deep-water corals in sclerochronology, Lethaia, 32, 119–130, 1999.

1131   Lin, I., Liu, W. T., Wu, C.-C., Wong, G. T. F., Hu, C., Chen, Z., Liang, W.-D., Yang, Y., and Liu, K.-K.: New
1132   evidence for enhanced ocean primary production triggered by tropical cyclone, Geophys. Res. Lett., 30,
1133   https://doi.org/10.1029/2003GL017141, 2003.

1134   Lorrain, A., Gillikin, D. P., Paulet, Y.-M., Chauvaud, L., Le Mercier, A., Navez, J., and André, L.: Strong
1135   kinetic effects on Sr/Ca ratios in the calcitic bivalve Pecten maximus, Geology, 33, 965–968, 2005.

1136   Lough, J. M.: Climate records from corals, WIREs Clim. Change, 1, 318–331,
1137   https://doi.org/10.1002/wcc.39, 2010.

1138   Madkour, H. A.: Distribution and relationships of heavy metals in the giant clam (Tridacna maxima) and
1139   associated sediments from different sites in the Egyptian Red Sea Coast, توزيع وعلاقات العناصر الثقيلة فى
1140   الكائن الصدفى الكبير)نراى داكنا مكسيما (والرواسب المصاحبة من مناطق مختلفة للساحل المصرى للبحر الاحمر, 2005.

1141   Mahé, K., Bellamy, E., Lartaud, F., and Rafélis, M. de: Calcein and manganese experiments for marking
1142   the shell of the common cockle (Cerastoderma edule): tidal rhythm validation of increments formation,
1143   Aquat. Living Resour., 23, 239–245, https://doi.org/10.1051/alr/2010025, 2010.

1144   Manasrah, R., Abu-Hilal, A., and Rasheed, M.: Physical and Chemical Properties of Seawater in the Gulf
1145   of Aqaba and Red Sea, in: Oceanographic and Biological Aspects of the Red Sea, edited by: Rasul, N. M.
1146   A. and Stewart, I. C. F., Springer International Publishing, Cham, 41–73, https://doi.org/10.1007/978-3-
1147   319-99417-8_3, 2019.

1148   Marin, F. and Luquet, G.: Molluscan shell proteins, Comptes Rendus Palevol, 3, 469–492,
1149   https://doi.org/10.1016/j.crpv.2004.07.009, 2004.

1150 Mat, A. M., Sarrazin, J., Markov, G. V., Apremont, V., Dubreuil, C., Eché, C., Fabioux, C., Klopp, C.,
1151 Sarradin, P.-M., Tanguy, A., Huvet, A., and Matabos, M.: Biological rhythms in the deep-sea
1152 hydrothermal mussel Bathymodiolus azoricus, Nat. Commun., 11, 3454,
1153 https://doi.org/10.1038/s41467-020-17284-4, 2020.

1154 Meibom, A., Stage, M., Wooden, J., Constantz, B. R., Dunbar, R. B., Owen, A., Grumet, N., Bacon, C. R.,
1155 and Chamberlain, C. P.: Monthly Strontium/Calcium oscillations in symbiotic coral aragonite: Biological
1156 effects limiting the precision of the paleotemperature proxy, Geophys. Res. Lett., 30,
1157 https://doi.org/10.1029/2002GL016864, 2003.

1158 Meyers, S. R.: Seeing red in cyclic stratigraphy: Spectral noise estimation for astrochronology,
1159 Paleoceanography, 27, 2012.

1160 Meyers, S. R.: Astrochron: An R package for astrochronology, http://cran.r-
1161 project.org/package=astrochron, 2014.

1162 Mohammed, T. A. A., Mohamed, M. H., Zamzamy, R. M., and Mahmoud, M. A. M.: Growth rates of the
1163 giant clam Tridacna maxima (Röding, 1798) reared in cages in the Egyptian Red Sea, Egypt. J. Aquat. Res.,
1164 45, 67–73, https://doi.org/10.1016/j.ejar.2019.02.003, 2019.

1165 Munro, J. L.: Estimation of the parameters of the von Bertalanffy growth equation from recapture data
1166 at variable time intervals, ICES J. Mar. Sci., 40, 199–200, https://doi.org/10.1093/icesjms/40.2.199,
1167 1982.

1168 Nassar, M. Z., Mohamed, H. R., Khiray, H. M., and Rashedy, S. H.: Seasonal fluctuations of phytoplankton
1169 community and physico-chemical parameters of the north western part of the Red Sea, Egypt, Egypt. J.
1170 Aquat. Res., 40, 395–403, https://doi.org/10.1016/j.ejar.2014.11.002, 2014.

1171 Nedoncelle, K., Lartaud, F., de Rafelis, M., Boulila, S., and Le Bris, N.: A new method for high-resolution
1172 bivalve growth rate studies in hydrothermal environments, Mar. Biol., 160, 1427–1439,
1173 https://doi.org/10.1007/s00227-013-2195-7, 2013.

1174 Onuma, N., Masuda, F., Hirano, M., and Wada, K.: Crystal structure control on trace element partition in
1175 molluscan shell formation, Geochem. J., 13, 187–189, 1979.

1176 Pandolfi, J. M. and Kiessling, W.: Gaining insights from past reefs to inform understanding of coral reef
1177 response to global climate change, Curr. Opin. Environ. Sustain., 7, 52–58,
1178 https://doi.org/10.1016/j.cosust.2013.11.020, 2014.

1179 Pannella, G.: Tidal growth patterns in recent and fossil mollusc bivalve shells: a tool for the
1180 reconstruction of paleotides, Naturwissenschaften, 63, 539–543, 1976.

1181 Petersen, S. V., Tabor, C. R., Lohmann, K. C., Poulsen, C. J., Meyer, K. W., Carpenter, S. J., Erickson, J. M.,
1182 Matsunaga, K. K., Smith, S. Y., and Sheldon, N. D.: Temperature and salinity of the Late Cretaceous
1183 western interior seaway, Geology, 44, 903–906, 2016.

1184 Poitevin, P., Chauvaud, L., Pécheyran, C., Lazure, P., Jolivet, A., and Thébault, J.: Does trace element
1185 composition of bivalve shells record utra-high frequency environmental variations?, Mar. Environ. Res.,
1186 158, 104943, https://doi.org/10.1016/j.marenvres.2020.104943, 2020.

1187 Polsenaere, P., Deflandre, B., Thouzeau, G., Rigaud, S., Cox, T., Amice, E., Bec, T. L., Bihannic, I., and
1188 Maire, O.: Comparison of benthic oxygen exchange measured by aquatic Eddy Covariance and Benthic
1189 Chambers in two contrasting coastal biotopes (Bay of Brest, France), Reg. Stud. Mar. Sci., 43, 101668,
1190 https://doi.org/10.1016/j.rsma.2021.101668, 2021.

1191 Popov, S. V.: Formation of bivalve shells and their microstructure, Paleontol. J., 48, 1519–1531,
1192 https://doi.org/10.1134/S003103011414010X, 2014.

1193 R Core Team: R: A language and environment for statistical   computing. R Foundation for Statistical
1194 Computing, 2013.

1195 Richard, M.: Analyse de la composition élémentaire de Pecten maximus par HR-ICP-MS Element 2:
1196 développements méthodologiques et interprétations écologiques., PhD Thesis, Université de Bretagne
1197 occidentale-Brest, 2009.

1198 Richardson, C. A., Crisp, D. J., Runham, N. W., and Gruffydd, L. D.: The use of tidal growth bands in the
1199 shell of *Cerastoderma edule* to measure seasonal growth rates under cool
1200 temperate and sub-arctic conditions, J. Mar. Biol. Assoc. U. K., 60, 977–989,
1201 https://doi.org/10.1017/S002531540004203X, 1980.

1202 Richter, C., Roa-Quiaoit, H., Jantzen, C., Al-Zibdah, M., and Kochzius, M.: Collapse of a new living species
1203 of giant clam in the Red Sea, Curr. Biol., 18, 1349–1354, 2008.

1204 Roa-Quiaoit, H.: Ecology and culture of giant clams (Tridacnidae) in the Jordanian sector of the Gulf of
1205 Aqaba, Red Sea, Httpelibsuubuni-BremendedissdocsE-Diss1340PHDROAQpdf, 2005.

1206 Roberts, E. M., Bowers, D. G., and Davies, A. J.: Tidal modulation of seabed light and its implications for
1207 benthic algae, Limnol. Oceanogr., 63, 91–106, https://doi.org/10.1002/lno.10616, 2018.

1208 Robson, A. A., Chauvaud, L., Wilson, R. P., and Halsey, L. G.: Small actions, big costs: the behavioural
1209 energetics of a commercially important invertebrate, J. R. Soc. Interface, 9, 1486–1498,
1210 https://doi.org/10.1098/rsif.2011.0713, 2012.

1211 Rodland, D. L., Schöne, B. R., Helama, S., Nielsen, J. K., and Baier, S.: A clockwork mollusc: Ultradian
1212 rhythms in bivalve activity revealed by digital photography, J. Exp. Mar. Biol. Ecol., 334, 316–323,
1213 https://doi.org/10.1016/j.jembe.2006.02.012, 2006.

1214 Sano, Y., Kobayashi, S., Shirai, K., Takahata, N., Matsumoto, K., Watanabe, T., Sowa, K., and Iwai, K.: Past
1215 daily light cycle recorded in the strontium/calcium ratios of giant clam shells, Nat. Commun., 3, 761,
1216 https://doi.org/10.1038/ncomms1763, 2012.

1217 Sather, W. A. and McCleskey, E. W.: Permeation and selectivity in calcium channels, Annu. Rev. Physiol.,
1218 65, 133–159, 2003.

1219 Savitzky, A. and Golay, M. J.: Smoothing and differentiation of data by simplified least squares
1220 procedures., Anal. Chem., 36, 1627–1639, 1964.

1221   Schöne, B. R. and Giere, O.: Growth increments and stable isotope variation in shells of the deep-sea
1222   hydrothermal vent bivalve mollusk Bathymodiolus brevior from the North Fiji Basin, Pacific Ocean, Deep
1223   Sea Res. Part Oceanogr. Res. Pap., 52, 1896–1910, 2005.

1224   Schöne, B. R. and Gillikin, D. P.: Unraveling environmental histories from skeletal diaries — Advances in
1225   sclerochronology, Palaeogeogr. Palaeoclimatol. Palaeoecol., 373, 1–5,
1226   https://doi.org/10.1016/j.palaeo.2012.11.026, 2013.

1227   Schöne, B. R., Castro, A. D. F., Fiebig, J., Houk, S. D., Oschmann, W., and Kröncke, I.: Sea surface water
1228   temperatures over the period 1884–1983 reconstructed from oxygen isotope ratios of a bivalve mollusk
1229   shell (Arctica islandica, southern North Sea), Palaeogeogr. Palaeoclimatol. Palaeoecol., 212, 215–232,
1230   2004.

1231   Schöne, B. R., Fiebig, J., Pfeiffer, M., Gleβ, R., Hickson, J., Johnson, A. L., Dreyer, W., and Oschmann, W.:
1232   Climate records from a bivalved Methuselah (Arctica islandica, Mollusca; Iceland), Palaeogeogr.
1233   Palaeoclimatol. Palaeoecol., 228, 130–148, 2005a.

1234   Schöne, B. R., Houk, S. D., Castro, A. D. F., Fiebig, J., Oschmann, W., Kröncke, I., Dreyer, W., and
1235   Gosselck, F.: Daily growth rates in shells of Arctica islandica: assessing sub-seasonal environmental
1236   controls on a long-lived bivalve mollusk, Palaios, 20, 78–92, 2005b.

1237   Schöne, B. R., Dunca, E., Fiebig, J., and Pfeiffer, M.: Mutvei's solution: An ideal agent for resolving
1238   microgrowth structures of biogenic carbonates, Palaeogeogr. Palaeoclimatol. Palaeoecol., 228, 149–166,
1239   https://doi.org/10.1016/j.palaeo.2005.03.054, 2005c.

1240   Schöne, B. R., Zhang, Z., Jacob, D., Gillikin, D. P., Tütken, T., Garbe-Schönberg, D., and SOLDATI, A.: Effect
1241   of organic matrices on the determination of the trace element chemistry (Mg, Sr, Mg/Ca, Sr/Ca) of
1242   aragonitic bivalve shells (Arctica islandica)—Comparison of ICP-OES and LA-ICP-MS data, Geochem. J.,
1243   44, 23–37, 2010.

1244   Schwartzmann, C., Durrieu, G., Sow, M., Ciret, P., Lazareth, C. E., and Massabuau, J.-C.: In situ giant clam
1245   growth rate behavior in relation to temperature: A one-year coupled study of high-frequency
1246   noninvasive valvometry and sclerochronology, Limnol. Oceanogr., 56, 1940–1951,
1247   https://doi.org/10.4319/lo.2011.56.5.1940, 2011.

1248   Service Hydrographique et Océanographique de la Marine - Géoportail:
1249   https://www.geoportail.gouv.fr/, last access: 28 June 2022.

1250   Sinclair, D. J., Kinsley, L. P. J., and McCulloch, M. T.: High resolution analysis of trace elements in corals
1251   by laser ablation ICP-MS, Geochim. Cosmochim. Acta, 62, 1889–1901, https://doi.org/10.1016/S0016-
1252   7037(98)00112-4, 1998.

1253   Soldati, A. L., Jacob, D. E., Glatzel, P., Swarbrick, J. C., and Geck, J.: Element substitution by living
1254   organisms: the case of manganese in mollusc shell aragonite, Sci. Rep., 6, 1–9, 2016.

1255   Soo, P. and Todd, P. A.: The behaviour of giant clams (Bivalvia: Cardiidae: Tridacninae), Mar. Biol., 161,
1256   2699–2717, https://doi.org/10.1007/s00227-014-2545-0, 2014.

1257 Surge, D., Lohmann, K. C., and Dettman, D. L.: Controls on isotopic chemistry of the American oyster,
1258 Crassostrea virginica: implications for growth patterns, Palaeogeogr. Palaeoclimatol. Palaeoecol., 172,
1259 283–296, 2001.

1260 Takesue, R. K., Bacon, C. R., and Thompson, J. K.: Influences of organic matter and calcification rate on
1261 trace elements in aragonitic estuarine bivalve shells, Geochim. Cosmochim. Acta, 72, 5431–5445, 2008.

1262 Tanaka, K., Okaniwa, N., Miyaji, T., Murakami-Sugihara, N., Zhao, L., Tanabe, K., Schöne, B. R., and Shirai,
1263 K.: Microscale magnesium distribution in shell of the Mediterranean mussel Mytilus galloprovincialis: An
1264 example of multiple factors controlling Mg/Ca in biogenic calcite, Chem. Geol., 511, 521–532,
1265 https://doi.org/10.1016/j.chemgeo.2018.10.025, 2019.

1266 Taylor, J. D. and Layman, M.: The mechanical properties of bivalve (Mollusca) shell structures,
1267 Palaeontology, 15, 73–87, 1972.

1268 Thébault, J., Chauvaud, L., L'Helguen, S., Clavier, J., Barats, A., Jacquet, Sé., PÉcheyran, C., and
1269 Amouroux, D.: Barium and molybdenum records in bivalve shells: Geochemical proxies for
1270 phytoplankton dynamics in coastal environments?, Limnol. Oceanogr., 54, 1002–1014,
1271 https://doi.org/10.4319/lo.2009.54.3.1002, 2009.

1272 Thébault, J., Jolivet, A., Waeles, M., Tabouret, H., Sabarot, S., Pécheyran, C., Leynaert, A., Jochum, K. P.,
1273 Schöne, B. R., Fröhlich, L., Siebert, V., Amice, E., and Chauvaud, L.: Scallop shells as geochemical archives
1274 of phytoplankton-related ecological processes in a temperate coastal ecosystem, Limnol. Oceanogr., 67,
1275 187–202, https://doi.org/10.1002/lno.11985, 2022.

1276 Thomson, D. J.: Spectrum estimation and harmonic analysis, Proc. IEEE, 70, 1055–1096, 1982.

1277 Tierney, J. E., Poulsen, C. J., Montañez, I. P., Bhattacharya, T., Feng, R., Ford, H. L., Hönisch, B., Inglis, G.
1278 N., Petersen, S. V., Sagoo, N., Tabor, C. R., Thirumalai, K., Zhu, J., Burls, N. J., Foster, G. L., Goddéris, Y.,
1279 Huber, B. T., Ivany, L. C., Turner, S. K., Lunt, D. J., McElwain, J. C., Mills, B. J. W., Otto-Bliesner, B. L.,
1280 Ridgwell, A., and Zhang, Y. G.: Past climates inform our future, Science, 370,
1281 https://doi.org/10.1126/science.aay3701, 2020.

1282 Tran, D., Nadau, A., Durrieu, G., Ciret, P., Parisot, J.-P., and Massabuau, J.-C.: Field chronobiology of a
1283 molluscan bivalve: how the moon and sun cycles interact to drive oyster activity rhythms, Chronobiol.
1284 Int., 28, 307–317, 2011.

1285 Tran, D., Perrigault, M., Ciret, P., and Payton, L.: Bivalve mollusc circadian clock genes can run at tidal
1286 frequency, Proc. R. Soc. B Biol. Sci., 287, 20192440, https://doi.org/10.1098/rspb.2019.2440, 2020.

1287 Vander Putten, E., Dehairs, F., Keppens, E., and Baeyens, W.: High resolution distribution of trace
1288 elements in the calcite shell layer of modern Mytilus edulis: Environmental and biological controls,
1289 Geochim. Cosmochim. Acta, 64, 997–1011, 2000.

1290 Vermeij, G. J.: The evolution of molluscan photosymbioses: a critical appraisal, Biol. J. Linn. Soc., 109,
1291 497–511, 2013.

1292 Von Bertalanffy, L.: Quantitative laws in metabolism and growth, Q. Rev. Biol., 32, 217–231, 1957.

1293 Warter, V. and Müller, W.: Daily growth and tidal rhythms in Miocene and modern giant clams revealed
1294 via ultra-high resolution LA-ICPMS analysis—A novel methodological approach towards improved
1295 sclerochemistry, Palaeogeogr. Palaeoclimatol. Palaeoecol., 465, 362–375, 2017.

1296 Warter, V., MÜLLER, W., WESSELINGH, F. P., TODD, J. A., and RENEMA, W.: LATE MIOCENE SEASONAL
1297 TO SUBDECADAL CLIMATE VARIABILITY IN THE INDO-WEST PACIFIC (EAST KALIMANTAN, INDONESIA)
1298 PRESERVED IN GIANT CLAMS, PALAIOS, 30, 66–82, https://doi.org/10.2110/palo.2013.061, 2015.

1299 Warter, V., Erez, J., and Müller, W.: Environmental and physiological controls on daily trace element
1300 incorporation in Tridacna crocea from combined laboratory culturing and ultra-high resolution LA-ICP-
1301 MS analysis, Palaeogeogr. Palaeoclimatol. Palaeoecol., 496, 32–47,
1302 https://doi.org/10.1016/j.palaeo.2017.12.038, 2018.

1303 Wassenburg, J. A., Scholz, D., Jochum, K. P., Cheng, H., Oster, J., Immenhauser, A., Richter, D. K., Häger,
1304 T., Jamieson, R. A., Baldini, J. U. L., Hoffmann, D., and Breitenbach, S. F. M.: Determination of aragonite
1305 trace element distribution coefficients from speleothem calcite–aragonite transitions, Geochim.
1306 Cosmochim. Acta, 190, 347–367, https://doi.org/10.1016/j.gca.2016.06.036, 2016.

1307 Wichern, N. M. A., de Winter, N. J., Johnson, A. L. A., Goolaerts, S., Wesselingh, F., Hamers, M. F., Kaskes,
1308 P., Claeys, P., and Ziegler, M.: The fossil bivalve Angulus benedeni benedeni: a potential
1309 seasonally resolved stable isotope-based climate archive to investigate Pliocene temperatures in the
1310 southern North Sea basin, EGUsphere, 1–53, https://doi.org/10.5194/egusphere-2022-951, 2022.

1311 Wilson, S. A., Koenig, A. E., and Orklid, R.: Development of microanalytical reference material (MACS-3)
1312 for LA-ICP-MS analysis of carbonate samples, Geochim. Cosmochim. Acta Suppl., 72, A1025, 2008.

1313 de Winter, N. J. and Claeys, P.: Micro X-ray fluorescence (µXRF) line scanning on Cretaceous rudist
1314 bivalves: A new method for reproducible trace element profiles in bivalve calcite, Sedimentology, 64,
1315 231–251, https://doi.org/10.1111/sed.12299, 2017.

1316 de Winter, N. J., Goderis, S., Dehairs, F., Jagt, J. W., Fraaije, R. H., Van Malderen, S. J., Vanhaecke, F., and
1317 Claeys, P.: Tropical seasonality in the late Campanian (late Cretaceous): Comparison between multiproxy
1318 records from three bivalve taxa from Oman, Palaeogeogr. Palaeoclimatol. Palaeoecol., 485, 740–760,
1319 2017.

1320 de Winter, N. J., Vellekoop, J., Vorsselmans, R., Golreihan, A., Soete, J., Petersen, S. V., Meyer, K. W.,
1321 Casadio, S., Speijer, R. P., and Claeys, P.: An assessment of latest Cretaceous Pycnodonte vesicularis
1322 (Lamarck, 1806) shells as records for palaeoseasonality: a multi-proxy investigation, Clim. Past, 14, 725–
1323 749, 2018.

1324 de Winter, N. J., Goderis, S., Malderen, S. J. M. V., Sinnesael, M., Vansteenberge, S., Snoeck, C., Belza, J.,
1325 Vanhaecke, F., and Claeys, P.: Subdaily-Scale Chemical Variability in a Torreites Sanchezi Rudist Shell:
1326 Implications for Rudist Paleobiology and the Cretaceous Day-Night Cycle, Paleoceanogr.
1327 Paleoclimatology, 35, e2019PA003723, https://doi.org/10.1029/2019PA003723, 2020.

1328 de Winter, N. J., Müller, I. A., Kocken, I. J., Thibault, N., Ullmann, C. V., Farnsworth, A., Lunt, D. J., Claeys,
1329 P., and Ziegler, M.: Absolute seasonal temperature estimates from clumped isotopes in bivalve shells
1330 suggest warm and variable greenhouse climate, Commun. Earth Environ., 2, 1–8,
1331 https://doi.org/10.1038/s43247-021-00193-9, 2021a.

1332 de Winter, N. J., Agterhuis, T., and Ziegler, M.: Optimizing sampling strategies in high-resolution
1333 paleoclimate records, Clim. Past, 17, 1315–1340, https://doi.org/10.5194/cp-17-1315-2021, 2021b.

1334 de Winter, N. J., Witbaard, R., Kocken, I. J., Müller, I. A., Guo, J., Goudsmit, B., and Ziegler, M.:
1335 Temperature Dependence of Clumped Isotopes (Δ47) in Aragonite, Geophys. Res. Lett., 49,
1336 e2022GL099479, https://doi.org/10.1029/2022GL099479, 2022.

1337 Winter, N. J. de, Sikkeleras, S. van, Goudsmit-Hazevoort, B., Boer, W., Nooijer, L. de, Reichart, G.-J.,
1338 Claeys, P., and Witbaard, R.: Tracing timing of growth in cultured mollusks using strontium spiking, 2022.

1339 Wisshak, M., Correa, M. L., Gofas, S., Salas, C., Taviani, M., Jakobsen, J., and Freiwald, A.: Shell
1340 architecture, element composition, and stable isotope signature of the giant deep-sea oyster
1341 Neopycnodonte zibrowii sp. n. from the NE Atlantic, Deep Sea Res. Part Oceanogr. Res. Pap., 56, 374–
1342 407, 2009.

1343 Witbaard, R., Jenness, M. I., Van Der Borg, K., and Ganssen, G.: Verification of annual growth increments
1344 in Arctica islandica L. from the North Sea by means of oxygen and carbon isotopes, Neth. J. Sea Res., 33,
1345 91–101, https://doi.org/10.1016/0077-7579(94)90054-X, 1994.

1346 Xing, Q., Zhang, L., Li, Y., Zhu, X., Li, Y., Guo, H., Bao, Z., and Wang, S.: Development of Novel Cardiac
1347 Indices and Assessment of Factors Affecting Cardiac Activity in a Bivalve Mollusc Chlamys farreri, Front.
1348 Physiol., 10, 2019.

1349 Yan, H., Shao, D., Wang, Y., and Sun, L.: Sr/Ca profile of long-lived Tridacna gigas bivalves from South
1350 China Sea: A new high-resolution SST proxy, Geochim. Cosmochim. Acta, 112, 52–65,
1351 https://doi.org/10.1016/j.gca.2013.03.007, 2013.

1352 Yan, H., Liu, C., An, Z., Yang, W., Yang, Y., Huang, P., Qiu, S., Zhou, P., Zhao, N., Fei, H., Ma, X., Shi, G.,
1353 Dodson, J., Hao, J., Yu, K., Wei, G., Yang, Y., Jin, Z., and Zhou, W.: Extreme weather events recorded by
1354 daily to hourly resolution biogeochemical proxies of marine giant clam shells, Proc. Natl. Acad. Sci., 117,
1355 7038–7043, https://doi.org/10.1073/pnas.1916784117, 2020.

1356 Yoshimura, T., Suzuki, A., Tamenori, Y., and Kawahata, H.: Micro-X-ray fluorescence-based comparison
1357 of skeletal structure and P, Mg, Sr, O and Fe in a fossil of the cold-water coral Desmophyllum sp., NW
1358 Pacific, Geo-Mar. Lett., 34, 1–9, 2014.

1359 Zhao, L., Schöne, B. R., and Mertz-Kraus, R.: Controls on strontium and barium incorporation into
1360 freshwater bivalve shells (Corbicula fluminea), Palaeogeogr. Palaeoclimatol. Palaeoecol., 465, 386–394,
1361 https://doi.org/10.1016/j.palaeo.2015.11.040, 2017.

1362

1363